EXPERIMENTAL AND NUMERICAL INVESTIGATION OF THE CRUSHING PROCESS OF COMPOSITE CRASH BOX

by

Mehmet Can ENGÜL

B.S., Mechanical Engineering, İzmir Institute of Technology, 2012

Submitted to the Institute for Graduate Studies in
Science and Engineering in partial fulfillment of
the requirements for the degree of
Master of Science

Graduate Program in Mechanical Engineering
Boğaziçi University
2016

EXPERIMENTAL AND NUMERICAL INVESTIGATION OF THE CRUSHING PROCESS OF COMPOSITE CRASH BOX

APPROVED BY:

Assoc. Prof. Nuri ERSOY . . . .
(Thesis Supervisor)

Assist. Prof. Sami And KILIÇ . . . .

Prof. Bülent EKİCİ . . . .

DATE OF APPROVAL: 02.09.2016

ACKNOWLEDGEMENTS

First and foremost, I would like to present my sincere gratitude to my supervisor Assoc. Prof. Nuri Ersoy. This thesis could not be possible without his patience, incomparable support, and unifying and completing touches to my study.

I am also thankful to my committee members, Assist. Prof. Sami And Kılıç and Prof. Bülent Ekici for their comments and constructive critics.

I also thank my friends and colleagues Fatih Ertuğrul Öz and Onur Yüksel for their assistance throughout the study.

I am grateful to Duygu Dalyanoğlu for opening a new door to me in the most critical period of my graduate program.

I would also like to express my appreciation to my friends Damla, İlker, Maral, Elif, Büşra, Ronay, Beril and Meltem for their all along mental and physical assistance with a neverending faith in me.

Last but definitely not the least, I am grateful to my father, Ercan Engül, my mother, Hülya Engül, my aunt, Deniz İyigünler and sisters, Dilşah Engül Sözeri and Pınar Engül for their continued love, support and understanding.

ABSTRACT

EXPERIMENTAL AND NUMERICAL INVESTIGATION OF THE CRUSHING PROCESS OF COMPOSITE CRASH BOX

Due to restrictions to bring down fuel consumption and carbon emissions, the recent research and technology innovations are encouraging automakers to apply new materials in automotive industry for light weight designs. Composites are being increasingly used in the industry because of their benefits over traditional metallic materials including their strength, weight, and reduction in manufacturing time. Along with these benefits, composites also have excellent performance related to energy absorption during impact and crash events. However, due to pressure for price limitations, the studies on applying composite materials mostly concentrate on the high priced elements per unit mass and the parts having significance in security. Crash box is the most distinct part that has those conditions.

The fracture process in composite structures is quite complex which involves not only intralaminar failure modes, but also interlaminar failure. Advances in commercial Finite Element Analysis (FEA) software have enabled engineers to realistically simulate the performance of composite components including these failure modes.

The thesis work will examine the modelling of crash behaviour of lightweight composite crash boxes in ABAQUS. A benchmarking study is applied to understand the modelling of the intralaminar damage mechanisms with 2D Hashin damage criteria and the delamination with decohesion elements which is called Cohesive Zone Modelling. Moreover, a new crash composite structure has been proposed, manufactured and tested and the results of the Finite Element simulation are compared to experimental results.

ÖZET

KOMPOZİT ÇARPIŞMA KUTULARININ EZİLME SÜRECİNİN DENEYSEL VE HESAPLAMALI OLARAK İNCELENMESİ

Karbon emisyonlarının azaltılması yönündeki baskı otomotiv üreticilerine araçlarda hafifletme çalışması yapmaları yönünde bir teşvik sağlamaktadır. Kompozit malzemeler, çelik ve diğer metalik malzemelerle karşılaştırıldığında, hafif olmaları, yüksek özgül dayanımları ve aynı zamanda yüksek tokluk ve mukavemetleri nedeniyle giderek artan uygulama alanlarına ve kullanım miktarına sahip olmaktadır. Öte yandan Kompozit malzemeler enerji soğurma kapasiteleri ve sönümleme özellikleri yüksek malzemelerdir. Ancak fiyat baskısı nedeniyle kompozit malzemelerin otomotiv pazarına girişi sınırlı olmaktadır. Bu nedenle otomotivde kompozit kullanımı üzerine yapılan çalışmalar, birim ağırlık başına fiyatı yüksek olan ve güvenlik açısından önem arz eden elemanlar üzerinde yoğunlaşmaktadır. Çarpışma kutusu bu şartlara sahip en belirgin parçadır.

Kompozit malzemelerde lamina içi ve aynı zamanda delaminasyonu içeren hasar mekanizmaları oldukça karmaşıktır. Günümüzde sonlu elemenlar metodu ile kompozit malzemelerin performansı gerçekçi olarak simüle edilebilmektedir.

Bu çalışma kapsamında, ağırlığı düşük kompozit çarpışma kutularının ezilme davranışı ABAQUS’te incelenmiştir. Modelin doğruluğunu teyid etmek için bir kıyaslama çalışması yapılmış, iç hasar mekanizmaları için Hashin kriteri kullanılırken, delaminasyon için yapışkan yüzeyler modeli uygulanmıştır. Ayrıca, yeni bir geometri tasarlanmış, deneysel ve hesaplamalı olarak incelenmiştir. Nümerik tahminler deney sonuçları ile karşılaştırılmıştır.

TABLE OF CONTENTS

LIST OF FIGURES

LIST OF TABLES

LIST OF SYMBOLS

°C	Celsius
C_d	Damaged elasticity matrix
d_m	Damage variable of matrix material
d_f	Damage variable of fibre material
d_s	Damage variable of shear factor
E_{11}	Elastic modulus in fibre direction
E_{22}	Elastic modulus in transverse direction
E_{33}	Elastic modulus through thickness
E_s	Spesific energy absorption
G_c	Fracture toughness
G_{ic}	Critical energy release rate under Mode- loading
GPa	Gigapascal
Gij	In-plane shear modulus
K	Interface stiffness
MPa	Megapascal
mm	Millimeter
W	Total absorbed energy
ε_{11}	Fibre direction strain
ε_{22}	Transverse direction strain
γ_{12}	Shear strain
υij	Poisson's ratios
Δ	Crush distance

LIST OF ACRONYMS / ABBREVIATIONS

ASTM	American Society for Testing and Materials
CFRP	Carbon-Fiber-Reinforced Polymer
CZM	Cohesive Zone Model
EU	European Union
FEA	Finite Element Analysis
MRCC	Manufacturer Recommended Cure Cycle
SEA	Spesific Energy Absorption

1. INTRODUCTION

The automotive sector is under constant pressure to bring down fuel consumption and reduce greenhouse gases emissions, including carbon dioxide with an increase in safety requirements. The average emissions from a car are 150 grams of carbon per kilometre. The average total carbon emissions from a car are 2,250 kilograms annually. In other words, 2,000 trees would need to be planted to offset the carbon emissions from a single car during its entire lifecycle. In the European Union (EU), CO_2 emissions restrictions will reduce passenger cars emission limits from 130g of CO_2/km today to a much more difficult to achieve target of 95g of CO_2/km in 2020 [1]. The most effective way of bringing down the fuel consumption is to reduce the automobile weight. In an automobile, every 45 kg weight reduction causes almost 3 per cent fuel saving [2]. As a result, the recent research and technology innovations are encouraging automakers to apply new materials in automotive industry for light weight designs.

Carbon fibre-reinforced or glass fibre-reinforced composites are not only light in weight but also stiff, strong and durable. The matrix resin properties and the type and orientation of the reinforcing material increase mechanical, chemical and thermal properties of the material greatly compared to other conventional materials. These advanced materials offer numerous new design possibilities for the components used in several sectors. For decades, the composites industry has witnessed steady growth, thanks notably to general economic development and the increased market penetration of this material in key markets, such as the construction, wind energy, aeronautics and automobile sectors.

Despite the improvements still being made with steel, and the increasing use of aluminium, the industry is looking at composite materials as a body material for high-volume applications. Composite materials have a large potential due to their superior properties and almost endless usage area. Composite components are some 30 to 50 per cent lighter in contrast to metal components. These composites thus contribute to a reduction in the carbon footprint and a favourable total cost of ownership [1]. Advanced plastics and polymer composites have being used in automotive industry in order to improve the appearance, functionality, and safety of automobiles while also reducing vehicle weight and delivering superior value to customers. In 2013, there is an increase of 8.8% in the demand for composites in the U.S. automotive market. Figure 1.1 demonstrates the percentage of composite penetration to the automotive industry from 1980 to 2020.

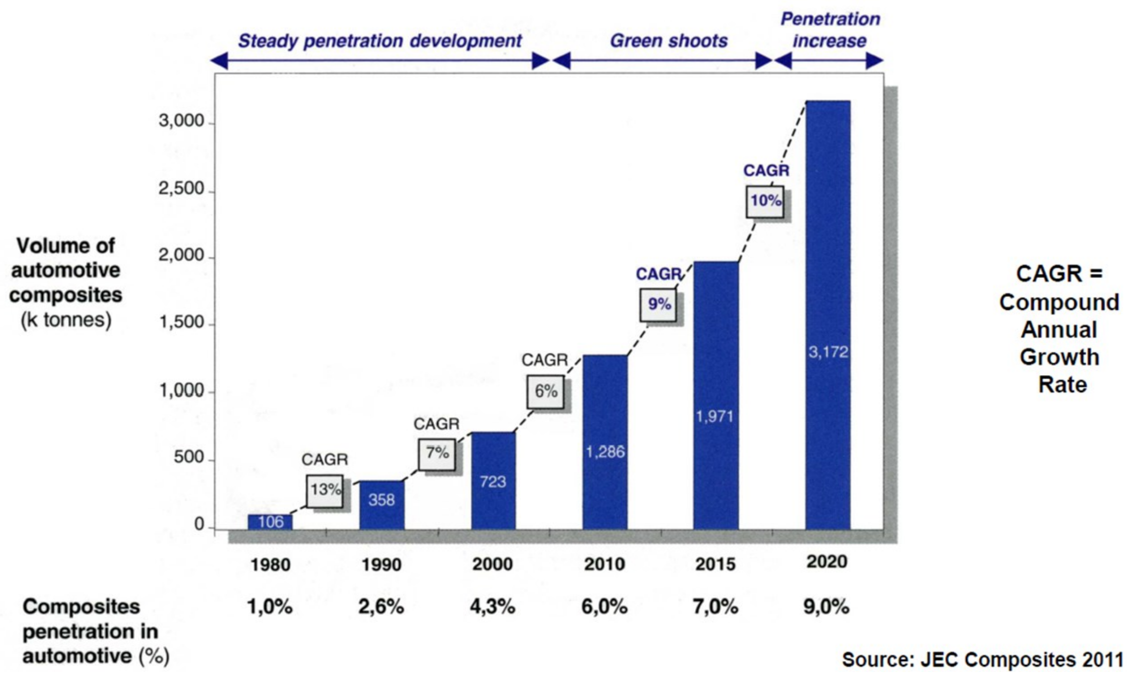

Figure 1.1. The volume and annual growth rate of composite penetration to the automotive industry [1].

Although there is a demand for increasing their usage, composite materials, due to price pressure, can be used mostly for parts which have low production rates such as wheels, seat backs and crumple zones in luxurious, sport and industrial vehicles. That is why, the studies on applying composite materials in automotive industry concentrate on the high priced elements per unit mass and the parts having significance in security. Crash box is the most distinct part that has those conditions. Figure 1.2 shows the crash box component in the frontal bumper system.

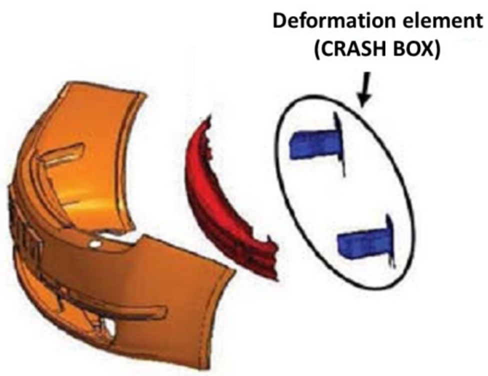

Figure 1.2. Frontal bumper system components [21].

It is known that there has been a steady increase in the number of studies and new designs to increase the vehicle security. However, according to statistics, in 2015, 7530 passenger vehicle occupants have lost their lives in crashes on Turkey roads [42]. About half of the deaths occur in frontal crashes [4]. Thus, the investigations concentrate mostly on improving the crashworthiness of vehicles [5-12]. The crashworthiness is protection level of the occupants of vehicle in a crash and depends on the rate of impact energy absorption and extinction. Crash box, which is equipped at the front end of its front side frame, is expected to collapse with absorbing crash energy prior to the other body parts in case of frontal crash so that the damage of the main cabin frame is minimized and passengers saved their lives [11].

Composite materials provide great potential for absorbing the energy of a crash event and reducing the accompanying accelerations and forces. Energy-absorbing composite components, which are usually designed to dissipate kinetic energy under controlled collapse or disintegration, substantially increase structural crashworthiness in exchange for a reasonable increase in overall vehicle cost. Figure 1.3 demonstrates the specific energy absorption capacity of various materials [20]. Several types of composite materials have greater capacity of energy absorption on a per unit mass basis, as compared to more commonly used metals, such as steel and aluminium. Hence, composites offer the potential to be used as very efficient energy-absorbing crash structures in automotive vehicles.

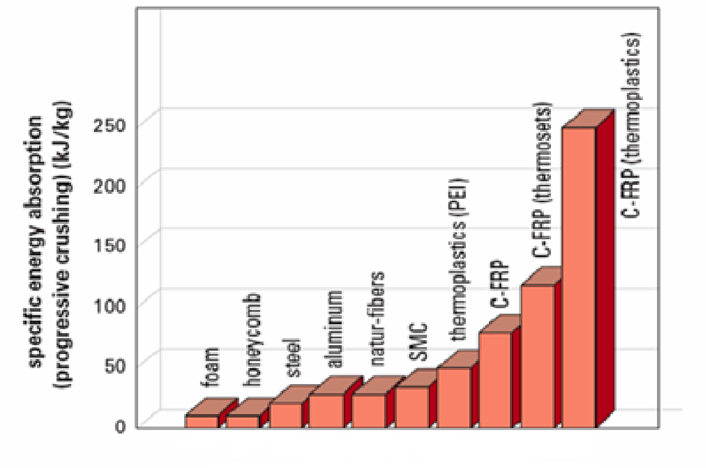

Figure 1.3. Specific energy absorption capacities for various materials [20].

In case of crash, metallic structures have high plastic deformation mechanisms such as plastic buckling and bending. Unlike metals, the main failure modes of fibre-reinforced composites are delamination, matrix compressive failure, matrix tensile failure, fibre compressive failure and fibre tensile failure. Energy is mainly absorbed by delamination. The fracture mechanisms of composites depend on the fracture time, geometry, material properties, and stacking sequence. By optimizing these parameters, it is possible to design composite structures with high energy absorbance capacities.

Thermoset composites have already been widely in use for many years. Thermoset composite production is characterized by relatively low equipment and tooling costs, great flexibility, high-grade characteristics and considerable freedom of design. However, Thermosets don't have proven recycling track records. According to European Union's end-of-life vehicle (ELV) directive, 85 per cent, by weight, of the materials used in each car built for the 2015 model year and beyond must be reusable or recyclable. Such requirements are feasible when long fibre thermoplastics are used [1].

Traditionally, the development of crashworthiness design relies upon experimental testing. When several loading directions are involved, the experimental testing of the crushing process in composites is rather costly. In addition, it is difficult to carry out a meaningful experimental program during the initial design stages and time required for completing the design is quite long. In automotive sector, it is required to decrease development times that consists design, production and testing periods. An alternative solution is the use of advanced computational tools such as Finite Element Analysis (FEA). FEA is a computerized method for predicting how a product reacts to real-world forces, vibration, heat, fluid flow, and other physical effects. Finite element analysis shows whether a product will break, wear out, or work the way it was designed. It is called analysis, but in the product development process, it is used to predict what is going to happen when the product is used. FEA works by breaking down a real object into a large number (thousands to hundreds of thousands) of finite elements, such as little cubes. Mathematical equations help predict the behaviour of each element. A computer then adds up all the individual behaviours to predict the behaviour of the actual object. FEA's main advantage is that it produces a much more detailed set of results than experimental investigations and is often quicker and less expensive.

1.1. Literature Review on Crash Studies for Composites

The progressive crush analyses for the various composite structures investigated the crushing behaviour of those structures occurring over a wide range of crushing speeds, in order to assess energy absorbing characteristics of those structures. The response of composite tubes under axial compression was earlier investigated experimentally in the study of Hull [13]. Hull showed that fibre arrangement appeared to have the greatest effect on the specific energy in the desired progressive crushing mode. Farley [14] investigated energy absorption characteristics of composite tubes in comparison with aluminium tubes by conducting static compression and impact tests. Farley demonstrated in an experimental work that the energy absorption capabilities of composites are a function of crushing speed. Mamalis et al. [15] investigated the crash behaviour of square composite tubes subjected to static and dynamic axial compression experimentally. In their experiments, a stable progressive collapse mode associated with large amounts of crash energy absorbed and a mid-length collapse mode characterized by brittle fracture and catastrophic failure are observed.

Besides experimental studies, utilization of numerical methods using finite element codes for design become very attractive due to high cost of the experimental and physical testing. Mamalis et al. [15] used explicit LS-DYNA to simulate the crash response of square CFRP composite tubes and validated the simulations with experimental results. Hörmann and Wacker [16] also used the LS-DYNA explicit code to simulate thermoplastic crash boxes. El-Hagel et al. studied numerical analysis of the quasi-static axial crush behaviour of aluminium-composite hybrid tube containing filament wound E glass fibre reinforced epoxy over-wrap around an aluminium tube. A modified Chang–Chang failure model was used for the composite layers with ±45° stacking sequence [17]. Indermuehle et al. [18] studied two approaches in ABAQUS to simulate the performance of composite cone structure including the common failure modes of delamination, fracture, and matrix damage. First they implemented a continuum damage mechanics approach using the constitutive model in ABAQUS/Explicit using a VUMAT user subroutine. The second approach is CZONE technology which is an empirically based approach where the behaviour of the composite is modelled through a "crush" material property. As an example for accurate results between test and simulations in ABAQUS, Sokolinsky et al. [19] simulates the crush behaviour of composite sine wave beam made of carbon/epoxy TORAYCA fabric. A continuum shell model was built in this study and the delamination is simulated by using cohesive zone modelling.

1.2. Problem Statement and Thesis Overview

Crash box is one of the significant parts of automobile due to high production price per unit mass and significance in security. Besides for applying new materials for light weight crash box designs, it is required to decrease development times for the design. A solution is the use of advanced computational tools such as Finite Element Analysis. That is why the crash behaviour and energy absorption capacity of composite materials has to be modelled by applying Finite Element Analysis. In the light of these points; for the thesis work, the modelling of crash behaviour in lightweight composite crash boxes is studied using the commercial software ABAQUS. For the intralaminar damage mechanisms such as transverse matrix cracking and fibre fracture, it is required to utilize some failure criteria. Since delamination is one of the predominant forms of failure for the case of crash simulation, in order to reach accurate results, not only intralaminar damage mechanisms but also interlaminar damage (delamination) has to be taken into consideration. That is why, for effective predictive capabilities, cohesive zone modelling (CZM) is adopted for failure analysis for delamination. CZM uses decohesion elements for the modelling of delamination. Decohesion elements use failure criteria that combine aspects of strength-based analysis to predict the onset of the softening process at the interface between laminae, and Fracture Mechanics to predict delamination propagation.

In addition, a benchmarking study of Sokolinsky's work [19] is reconstructed in order to understand the modelling of the intralaminar damage mechanisms and the delamination. Moreover, a new crash composite structure has been proposed, manufactured and tested and the results of the Finite Element simulation are compared to experimental results.

2. THEORY

2.1. Fibre Reinforced Polymers

Fibre-reinforced polymers (FRP), which are commonly used in the aerospace, automotive, marine, and construction industries, are composite materials made of a polymer matrix reinforced with fibres. The fibres are usually glass, carbon, or aramid. The polymer is usually a thermosetting resin such as epoxy, vinylester or polyester, or a thermoplastic resin such as polyamide (PA), polypropylene (PP) etc.

FRPs can be of single-layer or multi-layer type. The multi-layered composites are where several layers are stacked with fibres with orientation in different directions. Each layer can be unidirectional, where all fibres in that specific layer are aligned in one direction. They can also be woven, where the fibres have two or more directions. Different orientations provide different strengths and stiffness of the laminate.

In contrast to many other engineering materials, such as metals, composites are not isotropic. They are anisotropic in the sense that the properties (stiffness, strength, toughness etc.) differ in different directions. Layered FRPs are rather orthotropic, which means that properties are different in three perpendicular directions, which can be denoted as the longitudinal fibre direction, 1, transverse direction, 2, and the out-of-plane direction, 3, as depicted in Figure 2.1a. These directions are local to each ply in the stack-up. If the properties in the directions 2 and 3 are the same, the material is defined as transversely orthotropic. Fibre reinforced materials are most frequently used by employing multiple layers of material to form a laminate. Each thin layer may have a different fibre orientation as shown in Figure 2.1b.

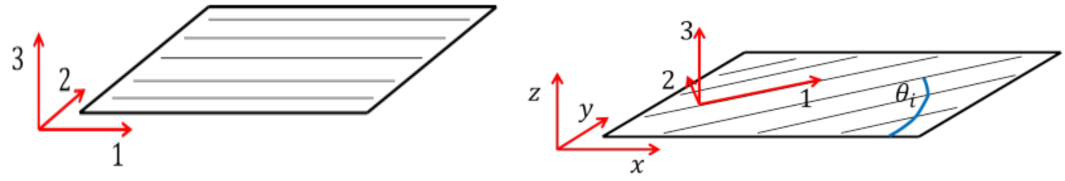

Figure 2.1. a) Illustration of how the orthotropic directions are defined, b) Illustration of how material orientation is related to coordinate systems [24]

2.2. Main Failure Modes of Composites

Several different failure modes can be observed when a composite material is subjected to a loading. The main failure modes of fibre-reinforced composites are delamination, matrix compressive failure, matrix tensile failure, fibre compressive failure fibre tensile failure and shear mode failure. Some explanation is required for each of these failure modes. Schematic Figures 2.2, 2.3, 2.4 and 2.5 show the matrix and fibre failure modes at different loadings [22, 23, 25].

Figure 2.2. Matrix failure modes. a) Shear matrix failure due to compression in transverse direction. b) Tensile matrix failure perpendicular to tensile load in transverse direction.

As illustrated in Figure 2.2a, when a composite fail in compressive matrix mode, the failure occurs due to the fibres and matrix crushing and interacting. The crack for this type of failure is most often at an angle to the loading direction. In contrast to compressive matrix failure, the fracture plane in tensile matrix failure is perpendicular to the loading as shown in Figure 2.2b [25]. Tensile matrix failure is generally due to a combination of three possible micromechanical failures: tensile failure of the matrix material, tensile failure of the fibre across its diameter, and failure of interface between the fire and matrix.

Figure 2.3. Fibre failure modes. (a) Shear fibre failure due to compression in fibre direction. (b) Tensile fibre failure perpendicular to tensile load in fibre direction.

If a composite is loaded in compression in the fibre direction as illustrated in Figure 2.3a, compressive fibre failure mode of fibre micro-buckling, which is also called shear mode, occurred since the matrix exhibits mostly shear strains. As a result of this mode kink bands occur to form.

Figure 2.3b shows the tensile failure in fibre direction. When fibres are loaded in longitudinal direction, fibres fail at low fracture strains and break in a brittle behaviour at their weakest cross sections. In addition, the energy absorption from fibre breakage when a composite fails is very low.

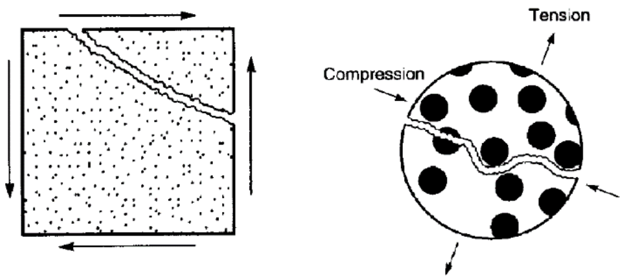

Figure 2.4. Failure in shear in the 2-3 plane [23]

For shear loading in 2-3 plane, since a shear stress produces a tensile stress on a plane oriented at 45°, performance of the material is limited by the matrix tensile failure, failure across the diameter of the fibre and failure of the interface between the fibre and matrix. Figure 2.4 illustrates these mechanisms as viewed in this shear mode. If the composite is loaded by shear stress in 1-2 plane, shear failure at interface is occurred as shown in Figure 2.5 [23].

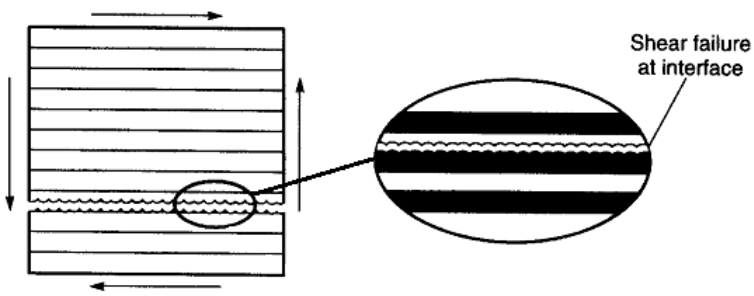

Figure 2.5. Failure in shear in the 1-2 plane [23]

When it comes to fracture mechanics and crash analysis one of the interesting characteristics is the amount of energy the material will be able to absorb. The energy is absorbed mainly by delamination. Delamination, the separation of two adjacent plies in composite laminates as given in Figure 2.6, represents one of the most critical failure modes in composite laminates. A delamination crack is often preceded by a crack which propagates through a ply until it has reached the fibres of an adjacent ply. Then the crack may branch off to go along the interface in between the plies, causing the delamination crack to form [27].

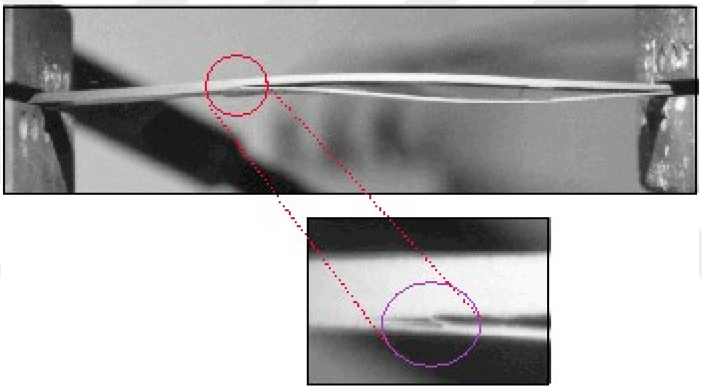

Figure 2.6. Delamination crack in specimen [26].

2.3. Crushing of Composites

When it comes to impact and crash events of structures, especially in vehicle applications, it is significant to select a material that can absorb the energy required to achieve an impact at an acceptable level of deceleration. Since composite materials have excellent performance of energy absorption during a constant crush load, due to many different energy absorbing mechanisms, composites are useful in crashworthy applications.

According to crush tests performed on composites, in order to prevent catastrophic failure, such as buckling, long thin-walled structures should not be used and it is relevant to use chamfered edge as trigger where the crushing is initiated. According to observations, there are several progressive crushing modes of composites [29]. The fragmentation is one of these modes. In this mode, partial lamina bundles are formed by one or multiple short interlaminar and longitudinal cracks in wedge-shaped laminate cross section (see Figure 2.7). Fracturing of lamina bundles is the main energy absorption mechanism.

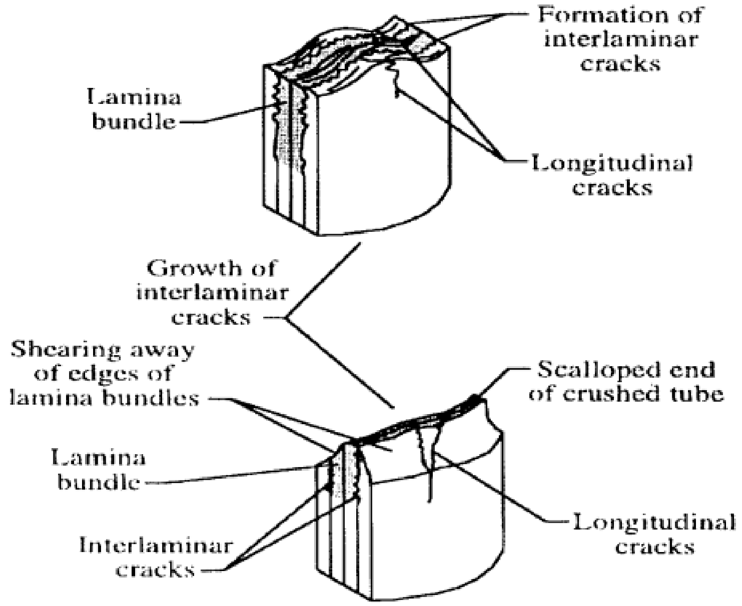

Figure 2.7. Fragmentation crushing mode [29].

Secondly, lamina bending or splaying mode can be seen in progressive crushing process as given in Figure 2.8. The splaying mode is characterized by very long interlaminar and intralaminar cracks which are the main energy absorbing mechanisms.

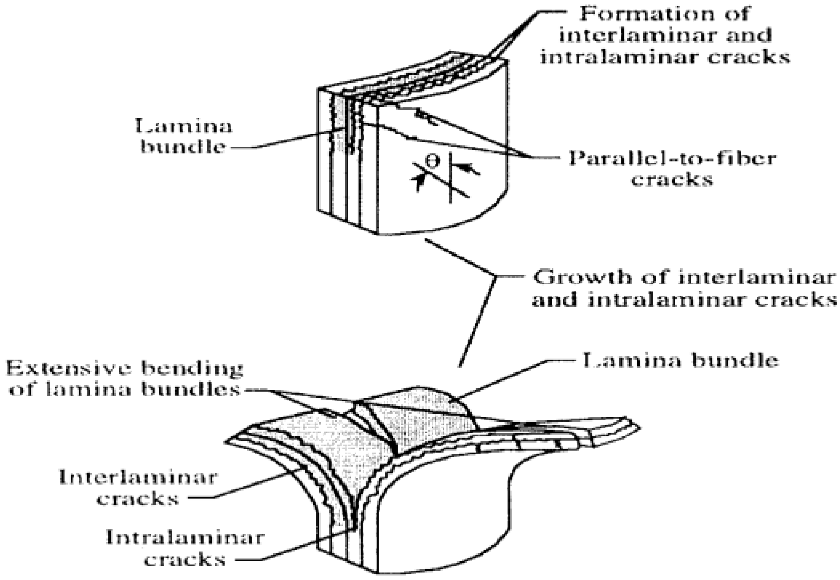

Figure 2.8. Splaying crushing mode [29].

In addition to fragmentation and splaying, the third mode is brittle fracturing. Figure 2.9 shows the brittle fracturing crushing mode which is a combination of fragmentation and splaying crushing modes. In brittle fracturing, energy is mainly absorbed by the fracturing of lamina bundles. On the other side, Figure 2.10 illustrates the local buckling or progressive folding mode. Formation of local buckles characterizes the progressive folding mode.

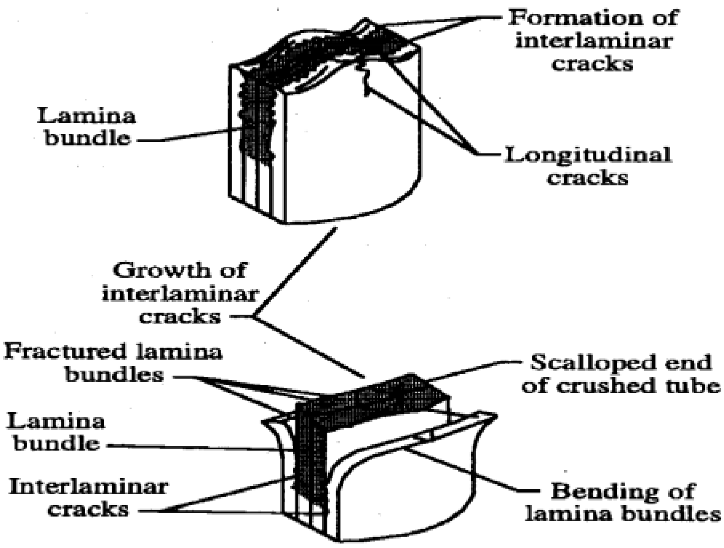

Figure 2.9. Brittle fracturing crushing mode [29].

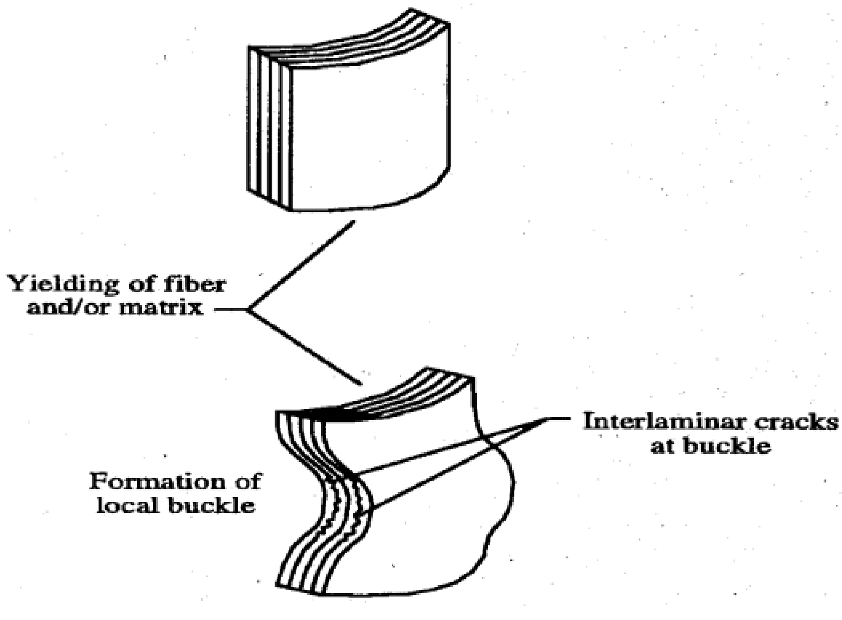

Figure 2.10. Local buckling crushing mode [29].

For detailed example of process, see Figure 2.11, a progressive behaviour of the crushing, triggered by a chamfered edge, is described at different stages for a cross-section of a tube with stack-up of $[90/0]_{2S}$ [28]. In the first stage the inner 90 layer is compressed and fails in shear and is forced to move inwards and then the middle axial layers come into contact with the rigid plate. Delamination also occurred at the centre as mode I delamination and between the 90^o and 0^o ply, will most likely as mode II delamination, which is a shearing mode. Finally, The outer 90^o layer will experience transverse shear cracks in the matrix due to compression and tensile stresses in its fibre direction, as the material is forced outwards [29].

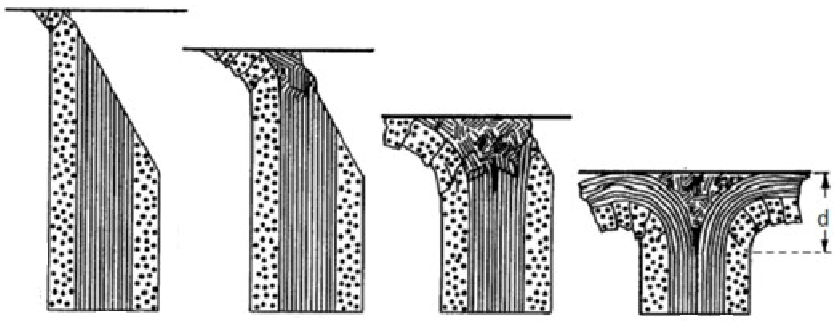

Figure 2.11. A schematic illustration of crushing of a tube with chamfered edge, modified from [28]

A typical force-displacement curve of axial crushing is given in Figure 2.12. There is an initial force peak, followed by stable crushing where the force remains at an almost constant level. The initial peak is higher because there have been no failure modes observed yet. The transition zone, the zone between the force peak and the stable crush zone, is highly dependent on how the crushing is triggered.

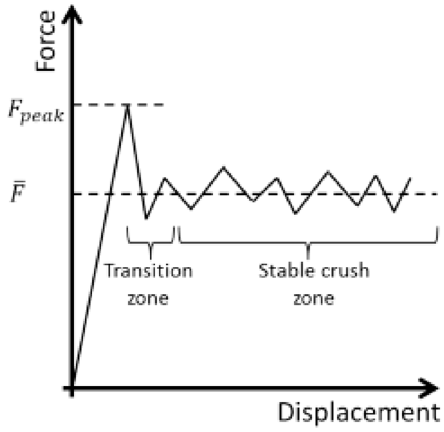

Figure 2.12. Typical force-displacement curve for a specimen subject to crushing [24].

The total energy, **W**, absorbed during process can be expressed according to Equation 2.1.

$$W = \int_0^{\Delta} F ds \tag{2.1}$$

where Δ is the crush distance and F is the measured force. The specific energy absorption, E_s can also be obtained, according to Equation 2.2, as the energy absorbed per unit mass. Along with material properties, specific energy absorption is also highly dependent of stacking sequence of plies and geometry of the crushing specimen.

$$E_s = \frac{W}{\rho A l} \tag{2.2}$$

where ρ is the density, A is the cross-sectional area, l is the crushed length. For crushing process, the specific energy absorption is a good value to use in comparison for different studies with different geometries and materials [24].

3. MODELLING PROGRESSIVE DAMAGE OF COMPOSITES IN ABAQUS

For conventional metallic structures, modern explicit FE codes are able to model the impact and crash energy absorbing mechanisms and are being successfully applied to simulate the collapse of these structures. This study is concerned with modelling the response of composite structures under impact loading.

Predicting failure in composites is quite complicated. In some cases composites may be able to sustain significantly larger load than that predicted by considerations of failure initiation alone (first ply failure). However, in order to fully exploit the design benefits of these materials, designers should be able to model the progressive damage growth. Each constituent of the composite materials fails progressively. Order of the failure of the constituents and ultimate stress and strain at failure is dependent upon the material type of fibre and matrix, layup sequence, volume fraction and other such manufacturing related parameters. Due to wide variety of types of composites, different progressive behaviour is obtained for each composite structure.

This section will discuss the progressive failure analysis of Fibre Reinforced Polymeric Composites (FRCP). For two dimensional analyses in ABAQUS, composite materials have two main failure mechanisms: in plane failure mechanisms (fibre and matrix failure) and delamination. Through thickness failure mechanisms are not taken into consideration.

3.1. Intralaminar Analysis

For Intralaminar failure analysis approach, strength based failure criteria is used. Strength-based failure criteria predict the onset of different damage mechanisms in a single ply of composite [30].

In order to understand the failure modelling capabilities, consider the stress-strain response of a hypothetical material during a simple tensile test, such as illustrated in Figure 3.1.

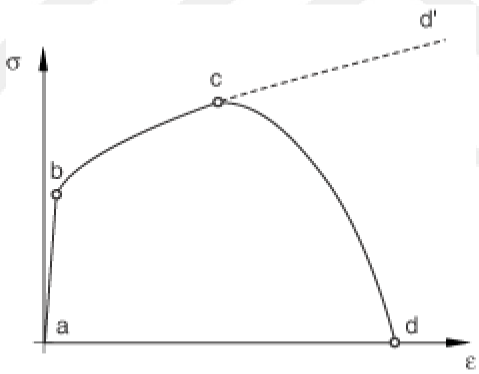

Figure 3.1. Typical uniaxial stress-strain response of a metal specimen.

Figure 3.1 shows distinct phases. The response of the undamaged material is assumed to be linearly elastic, a–b, and the model is intended to predict behaviour of fibre-reinforced materials for which damage can be initiated without a large amount of plastic deformation. That is why, plastic yielding with strain hardening, b–c, can be ignored. Point c identifies the material state at the onset of damage, which is referred to the damage initiation criterion. The last part, c–d, demonstrates the damage evolution law. The stress-strain response is governed by the evolution of the degradation of the stiffness in the region of strain localization. In the context of damage mechanics c–d can be viewed as the degraded response of the curve c–d'. The material would have followed in the absence of damage. Elements can be removed from the calculations once the material stiffness is fully degraded at point d.

The undamaged material response is specified by defining an orthotropic linear elastic material. For 2D plane stress conditions, the stress-strain relations for the in-plane components of the stress and strain are of the form as in Eq. 3.1.

$$\begin{Bmatrix} \varepsilon_1 \\ \varepsilon_2 \\ \gamma_{12} \end{Bmatrix} = \begin{bmatrix} 1/E_1 & -v_{12}/E_1 & 0 \\ -v_{21}/E_2 & 1/E_2 & 0 \\ 0 & 0 & 1/G_{12} \end{bmatrix} \begin{Bmatrix} \sigma_1 \\ \sigma_2 \\ \tau_{12} \end{Bmatrix} \tag{3.1}$$

In Eqn. 3.1, E_1 is the Young's modulus in the fibre direction, E_2 is the Young's modulus in the direction perpendicular to the fibres, G_{12} is the shear modulus, v_{12} and v_{21} are Poisson's ratios.

In ABAQUS, the two dimensional Hashin initiation criteria is used to predict the onset of damage, and the damage evolution law is based on the energy dissipated during the damage process and linear material softening.

3.1.1. Damage Initiation

Failure theory of anisotropic composite material was primarily used as an indication of failure initiation for each observed failure mode in the progressive failure methodology. Damage initiation is simply the point at which the material properties are first affected. Failure criteria theories for composites were principally established by extending the existing failure theories for isotropic materials to account for the anisotropic characteristics of composites in the strength. The intralaminar damage of composite can be classified into several basic types, such as longitudinal fibre tensile breakage, compressive buckling or kinking, transverse matrix cracking, etc., based on either equivalent stress or strain. Failure surface is defined by a set of polynomial equations in terms of two or three dimensional stress and strain quantities with adjustable parameters to be determined from test or numerical experiment.

There is large number of failure theories formulated for composite materials. The most widely applied theories on lamina level are Tsai-Hill theory (1965), Tsai-Wu theory (1971), Hashin and Rotem failure criteria (1973), Hashin 3D failure criteria (1980), Chang-Chang criteria (1987), Christensen failure criteria (1997) and Puck's criteria (1998). One of the recently applied studies is LaRC04 failure criterion which is proposed by Pinho et al. (2005).

ABAQUS has a built in Hashin failure criteria; that is why, it is investigated in the following section in detail.

3.1.1.1. Hashin Damage Initiation Criteria

In the study of Hashin [31], four different modes of failure are considered:

- Fibre rupture in tension,
- Fibre buckling and kinking in compression,
- Matrix cracking under transverse tension and shearing,
- Matrix crushing under transverse compression and shearing.

The failure modes included in Hashin's criteria are given with equations 3.2-3.5 as follows.

1. Tensile fibre failure for $\sigma_{11} \geq 0$

$$\left(\frac{\sigma_{11}}{X_T}\right)^2 + \alpha\left(\frac{\sigma_{12}}{S_L}\right)^2 \geq 1, \qquad \text{where } 0 \leq \alpha \leq 1 \tag{3.2}$$

2. Compressive fibre failure for $\sigma_{11} < 0$

$$\left(\frac{\sigma_{11}}{X_C}\right)^2 \geq 1 \tag{3.3}$$

3. Tensile matrix failure for $\sigma_{22} > 0$

$$\left(\frac{\sigma_{22}}{Y_T}\right)^2 + \left(\frac{\sigma_{12}}{S_L}\right)^2 \geq 1 \tag{3.4}$$

4. Compressive matrix failure for $\sigma_{22} < 0$

$$\left(\frac{\sigma_{22}}{2S_T}\right)^2 + \left[\left(\frac{Y_C}{2S_T}\right)^2 - 1\right]\frac{\sigma_{22}}{Y_C} + \left(\frac{\sigma_{12}}{S_L}\right)^2 \geq 1 \tag{3.5}$$

where, σ_{ij} denote the stress components and the tensile and compressive allowable strengths for lamina are denoted by subscripts T and C, respectively. X_T and Y_T denote the allowable tensile strengths in fibre and transverse directions respectively. Similarly, X_C and Y_C denote the allowable compressive strengths in fibre and transverse directions respectively. Further, S_L and S_T denote allowable longitudinal and transverse shear strengths.

3.1.2. Damage Evolution

Damage evolution criteria determines how the material behaves after damage has been initiated. Damage is characterized by the degradation of material stiffness. It plays an important role in the analysis of fibre-reinforced composite materials. Many such materials exhibit elastic-brittle behaviour; that is, damage in these materials is initiated without significant plastic deformation. Consequently, plasticity can be neglected when modelling behaviour of such materials [30].

The response of the material is computed from

$$\sigma = C_d\,\varepsilon \tag{3.6}$$

Where ε is the strain and C_d is the damaged elasticity matrix, which has the form

$$C_d = \frac{1}{D}\begin{bmatrix} (1-d_f)E_1 & (1-d_f)(1-d_m)v_{21}E_1 & 0 \\ (1-d_f)(1-d_m)v_{12}E_2 & (1-d_m)E_2 & 0 \\ 0 & 0 & (1-d_s)G_{12}D \end{bmatrix} \tag{3.7}$$

where $D = 1-(1-d_f)(1-d_m)v_{21}v_{12}$

where d_f reflects the current state of fibre damage, d_m reflects the current state of matrix damage, d_s reflects the current state of shear damage, E_1 is the Young's modulus in the fibre direction, E_2 is the Young's modulus in the direction perpendicular to the fibres, G_{12} is the shear modulus, and v_{12} and v_{21} are Poisson's ratios. Equations show how the stiffness of the material decreases as the values of the damage variables increase. Once a damage variable for an integration point reaches a value of 1, that point no longer contributes any strength or stiffness to the model and can be deleted. Matzenmiller et al. [38] point out that the normal stress contributions, induced by Poisson's ratio, are the first to be diminished that they are affected by both damage variables.

3.1.3 Damage Stabilization

Sometimes ABAQUS Standard can have difficulties converging while modelling damage growth with an implicit method [30]. To help with convergence, ABAQUS has a viscous regularization scheme which can be utilized. Four properties are required for the viscous regularization to be active. These are viscous coefficients for each of the four failure modes applied in damaged elasticity matrix given in section 3.1.2. A viscous damage variable is defined by the evolution equation (see Eqn. 3.7).

$$\dot{d}_v = \frac{1}{\eta}(d - d_v) \tag{3.8}$$

where η is the viscosity coefficient representing the relaxation time of the viscous system and d is the viscous damage variable.

In ABAQUS Explicit, viscous regularization can be used to model rate dependent material behaviour. It slows down the rate of damage growth and increases the fracture energy as deformation rates increase [30].

3.2. Interlaminar Analysis (Cohesive Zone Modelling)

The fracture process in composite structures is quite complex which involves not only intralaminar damage mechanisms (e.g. Transverse matrix cracking, fibre fracture), but also interlaminar damage (delamination). Delamination is one of the predominant forms of failure and especially for the case of crash simulation the energy is absorbed mainly by delamination process. That is why, for effective predictive capabilities, the failure analysis tools for different failure modes including delamination are required.

For single mode delamination analysis, Figure 3.2 represents the traction-separation behaviour of cohesive zone in specimens loaded in pure Modes I, II and III and constitutive behaviours. A penalty stiffness, K, is used to hold the top and bottom faces of the decohesion element together in the linear elastic range (Point 1 in Figure 3.2). For pure Mode I, II or III loading, after the interfacial normal or shear tractions attain their respective interlaminar tensile or shear strengths (Point 2 in Figure 3.2), delamination starts and the stiffness is gradually reduced to zero. The onset displacements (δ^o_1, δ^o_2 and δ^o_3) are obtained by dividing tensile or shear strengths to stiffness value. The area under the traction–relative displacement curves, named as fracture toughness (G_{IC}, G_{IIC} and G_{IIIC} respectively), defines the final relative displacements, δ^f_1, δ^f_2 and δ^f_3 (Point 4 in Figure 3.2). In shear modes, the traction-separation curves are symmetric, and same behaviour is expected when the direction of shear is inverted (Figure 3.2.a), and in tensile mode, no failure is expected in compression (Figure 3.2.b)

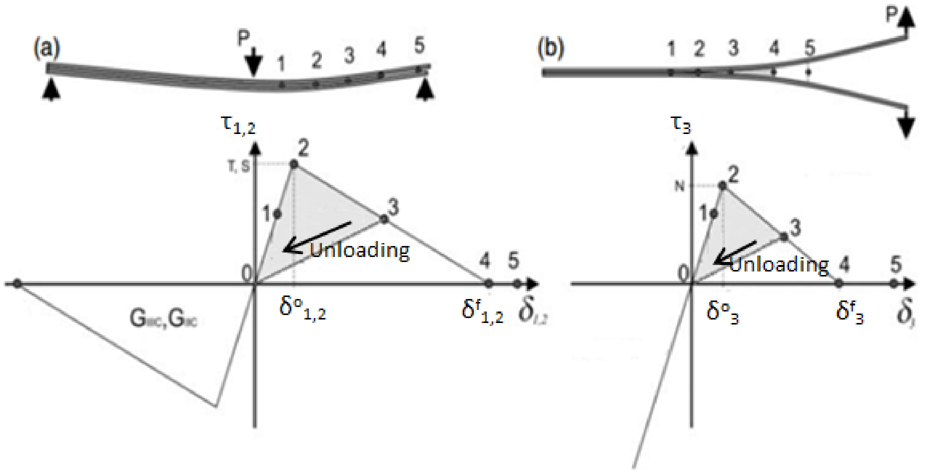

Figure 3.2. Pure mode constitutive equations: (a) Mode II or Mode III; (b) Mode I.

In structural applications of composites, instead of single mode analysis, delamination growth is likely to occur under mixed-mode loading. Therefore, a general formulation for decohesion elements dealing with mixed-mode delamination onset and propagation is also required [32]. Decohesion elements use failure criteria that combine aspects of strength-based analysis to predict the onset of the softening process at the interface between laminae, and Fracture Mechanics to predict delamination propagation. Camanho et al. [33], developed zero-thickness volumetric decohesion elements able to capture delamination onset and growth under mixed-mode loading conditions in composite structural components.

For the Cohesive Zone Modelling in ABAQUS, carrying out the theory and formulations are quite important to apply precise model.

3.2.1. Formulations of Cohesive Zone Modelling

Some studies investigate formulations about delamination and their applications to composite structures [33-37]. In this part, these formulations are described which are also included in ABAQUS for CZM.

Cohesive damage zone models relate cohesive surface tractions, σ , to separation, Δ, at an interface where a crack may occur. The law used in this paper is a bilinear relation between the traction and the separation (see Figure 3.3) [37]. Damage initiation is related to the interfacial strength, σ_c , i.e., the maximum traction on the traction–separation relation. The area under the traction–separation relation is equal to the fracture toughness, G_c.

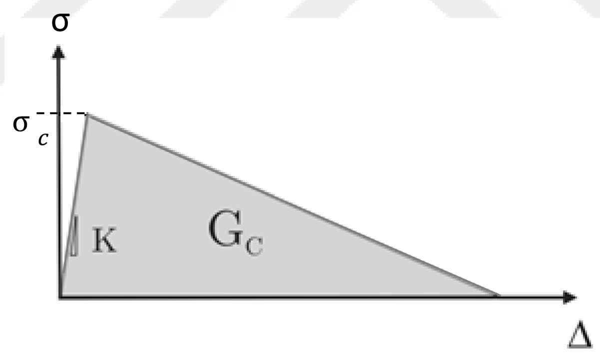

Figure 3.3. Bilinear constitutive equation [37]

According to Figure 3.3, Relative displacement at damage initiation, Ɛ,,is defined in Eq. (3.8).

$$\varepsilon_c = \frac{\sigma_c}{K} \tag{3.8}$$

$$\sigma_c = E_3\, \varepsilon_c = K\Delta \tag{3.9}$$

K is the interface stiffness that relates the resulting tractions at the interface with the opening displacement, Δ and E_3 is the through-the-thickness Young's modulus of the material. The effective strain of the composite is shown in Eqn. 3.10.

$$\varepsilon_{eff} = \frac{\delta t}{t} + \frac{\Delta}{t} = \varepsilon + \frac{\Delta}{t} \tag{3.10}$$

where t is the thickness of each ply.

By converting ε to E, the equivalent Young's modulus can be written as a function of the Young Modulus of the material. Using Eqns. (3.9) and (3.10), the effective Young's modulus is written as in Eq. (3.11).

$$E_{eff} = E_3 \left(\frac{1}{1 + \frac{E_3}{Kt}} \right) \tag{3.11}$$

The effective elastic properties of the composite will not be affected by the cohesive surface if $E_i \ll K_i t$. At that point a parameter m is defined and Eq. (3.12) is obtained. Equations (3.8) and (3.12) can be applied for each single crack modes shown in Table 3.1.

$$K_i = \frac{mE_i}{t} \tag{3.12}$$

Interface stiffness, K, should be large enough to provide a reasonable stiffness but small enough to reduce the risk of numerical problems such as spurious oscillations of the tractions. According to the study of Turon et al [37], m is taken as 50 since the loss of stiffness due to presence of interface for that m value is sufficiently accurate for problems.

Table 3.1. Equations for each single mode.

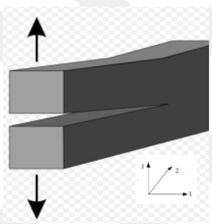	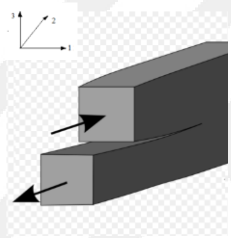	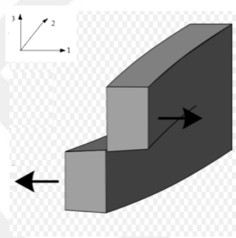
MODE I (Opening)	MODE II (In-plane shear)	MODE III (Out-of-plane shear)
$\varepsilon_3 = \frac{\sigma_{33}}{K_I}$	$\varepsilon_{31} = \frac{\tau_{31}}{K_{II}}$	$\varepsilon_{32} = \frac{\tau_{32}}{K_{III}}$
$K_I = \frac{mE_{33}}{t}$	$K_{II} = \frac{mG_{31}}{t}$	$K_{III} = \frac{mG_{32}}{t}$

The damage initiation can be calculated by quadratic formula of Eq. (3.13). In this model, linear softening damage law, shown in Figure 3.3, is used with the mixed-mode fracture energy criteria based on Power law (Eq. (3.14)).

$$\left(\frac{\sigma_{I}}{\sigma_{Ic}}\right)^{2}+\left(\frac{\sigma_{II}}{\sigma_{IIc}}\right)^{2}+\left(\frac{\sigma_{III}}{\sigma_{IIIc}}\right)^{2}=1 \qquad (3.13)$$

$$\left(\frac{G_{I}}{G_{I}^{c}}\right)^{\propto}+\left(\frac{G_{II}}{G_{II}^{c}}\right)^{\propto}+\left(\frac{G_{III}}{G_{III}^{c}}\right)^{\propto}=1 \qquad (3.14)$$

where G_I^c is normal fracture energy, G_{II}^c and G_{III}^c are shear fracture energies for Mode-II and Mode-III respectively. G_I is the normal strain energy release rate, G_{II} and G_{III} are shear strain energy release rates for Mode-II and Mode-III respectively.

The viscosity parameter is required to be defined for stability in solving the nonlinear equations. It is difficult to achieve the nonlinear iteration convergence without this parameter. As this slightly affects the CPU time but not the results, values from 10^{-5} to 10^{-3} were recommended. In the model of Chen et al [34] an optimum value of 10^{-4} is chosen. Besides stiffness and viscosity parameters, a friction coefficient, which describes the frictional forces between the surfaces separated, has also to be set in order to calibrate cohesive law. Friction coefficient, mostly determined by experimental studies, is used in this study as the value indicated in the study of Sokolinsky et. al. [19]

4. NUMERICAL ANALYSIS

For Numerical Analysis, commercial finite element program ABAQUS/Explicit is used to simulate the behaviour of the crash boxes during crash tests. When compared to the implicit methods, explicit FE methods are better in solving structural problems involving complex contact interactions occurring within a short duration.

Simulations of crushing processes can be carried out in quasi-static and impact conditions. In impact conditions, the structure is subjected to decrease in crush speed, from an initial impact speed to final rest, which is true behaviour of the actual crush. In quasi-static compression, the specimen is crushed at a constant speed. Since energy absorption capability is dependent on the speeds, quasi-static analysis may not be a true simulation of the actual crash condition. However, quasi static simulations are time-effective and easy to control. That is why; quasi-static modelling is mostly preferred in the studies of progressive failure analysis [29].

This part presents, firstly, the case study of simple delamination model to apply cohesive zone method. Then, the benchmark study and the numerical analysis of a novel geometry are proposed. Since the quasi-static modelling is applied in benchmark study and impact testing of novel geometry is difficult for the crushing unless provided with expensive equipment, in this study, crushing simulations for all specimens are carried out in quasi-static conditions.

4.1. Case Study: Simple Model for Delamination with CZM in ABAQUS

According to the CZM equations, in order to see the delamination behaviour, CRFP sample with the stacking sequence of $(0/90)_{2s}$ and ply thickness of 0.125 mm under impact loading is modelled in ABAQUS. Each ply is extruded in 2D separately and bonded with the interaction module by assigning interlaminar cohesion parameters. Interlaminar cohesion parameters are taken from the study of Sokolinsky et al. [19]. Table 4.1 shows the interlaminar strength and fracture energy values of the material. Interface stiffness values are calculated as indicated in Eq. (3.12), where m is taken as 50. Friction coefficient between cohesive elements is chosen as 0.2 in this case study. To initiate delamination properly, crushed surface is 45^o chamfered. The specimen can be seen in Figure 4.1.

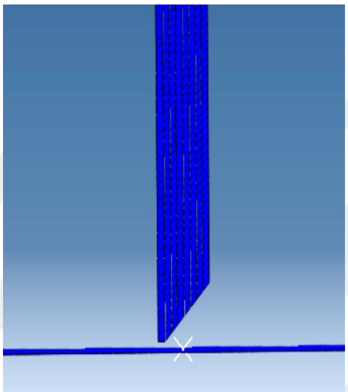

Figure 4.1. The two-dimensional specimen.

For the prediction of α value in the power law fracture energy criteria formula, Chen et al. compares the predicted failure loads for α=1 and α=2, to the experimental results [34]. Chen obtained that there is a good agreement between prediction and the tested failure results when α is equal to 1. That is why, fracture energy criteria based on Power Law formulation is applied with α=1.

Table 4.1. Interlaminar material strength and fracture energy values

σ_{33c} (MPa)	σ_{13c} (MPa)	σ_{23c} (MPa)	G_I^c(J/m^2)	G_{II}^c(J/m^2)	G_{III}^c(J/m^2)
54	70	70	504	1566	1566

Finally, element deletion is applied according to Hashin failure criteria where following conditions is provided.

- Hashin Matrix compressive failure criteria > 0.99
- Hashin Fibre Compressive Failure criteria> 0.99

4.2. Benchmark Study

The study of Sokolinsky et al. [19] presents a physics-based finite element model of a sine wave shape carbon–epoxy fabric composite plate subject to quasi-static crushing that consists intralaminar (in-plane) and interlaminar (delamination) failure mechanisms in ABAQUS/Explicit. In this work, the finite element model of Sokolinsky et al. is reapplied in ABAQUS/Explicit for the validation of the numerical methodology. View of the model is given in Figure 4.2.

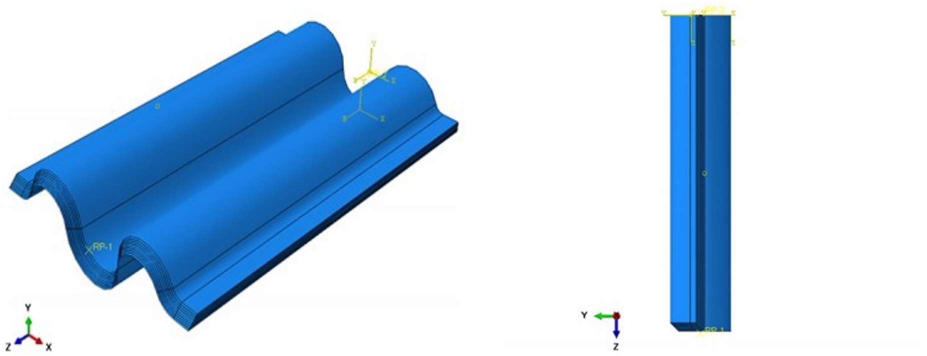

Figure 4.2. The top and side view of the ABAQUS/CAE model of the composite plate

As modelled specimen, the $[0/90]_{2S}$ composite lay-up is 2 mm thick and 76.2 mm long. A single-sided 45-degree chamfer is applied at the bottom of the specimen that is accounted as crush initiator. The cross-section of the corrugated plate specimen can be obtained by repeating a semi-circular segment of radius 6.35 mm three times at alternating sides with respect to the mid-plane (see Figure 4.3).

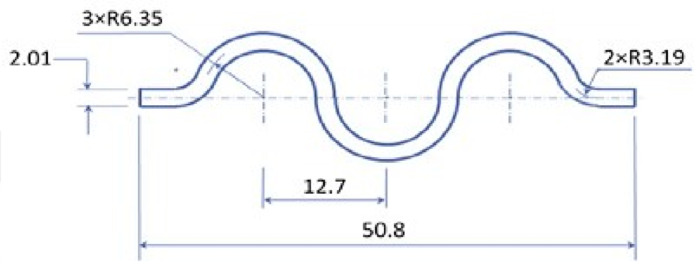

Figure 4.3. Cross-sectional view of the plate (All dimensions are given in mm.)

Both intralaminar (in-plane) and interlaminar (delamination) failure mechanisms are considered in order to simulate the real physics of composites crushing. The in-plane response of the composite plies is modelled with the Hashin damage criteria as a homogeneous orthotropic material which is capable of sustaining progressive stiffness degradation due to fibre/matrix cracking. This model requires the density value, elasticity constants, damage initiation coefficients and damage evolution coefficients. The elasticity constants include the Young's modulus in the fibre directions, the principal Poisson's ratio, and the in-plane shear modulus. The damage initiation coefficients include the tensile and compressive strengths along the fibre directions and the shear strength at the onset of shear damage. The values of the user material constants and damage initiation coefficients are given in Table 4.2. Interlaminar response of the plate is modelled according to cohesive zone modelling approach as validated in simple delamination model. The used cohesion parameters were previously given in Table 4.1.

Table 4.2. Material Properties of TORAYCA T700/2510 [39]

Description	Variable	Value
Density [g/cm3]	ρ	1.53
Longitudinal modulus [GPa]	E_{11}	55.9
Transverse modulus [GPa]	$E_{22}=E_{33}$	54.4
Principal Poisson's Ratio	v_{12}	0.42
Shear Moduli	$G_{12}=G_{23}=G_{31}$	4.2
Longitudinal Tensile Strength [MPa]	X_{1+}	911.3
Longitudinal Compressive Strength [MPa]	X_{1-}	704
Transverse Tensile Strength [MPa]	Y_{2+}	770
Transverse Compressive Strength [MPa]	Y_{2-}	698.2
In-plane Shear Strength [MPa]	S	131.6

Each of the eight fabric plies were individually meshed with continuum shell elements (SC8R). Continuum shell elements in ABAQUS have the geometry of a three-dimensional solid element but their kinematic and constitutive behaviours are similar to those of conventional shell elements. As pointed in the study of Sokolinsky et al., the crushing load was applied to the composite plate through another rigid steel plate moving with a constant velocity of 200 mm/s. The friction coefficient between the surfaces of the debonded composite plies was assumed to be 0.3 [19].

4.3. Numerical Analysis of Composite Specimen with a Novel Geometry (Sandwich Structure)

This section contains the numerical analysis of composite crash box structure where a novel geometry is proposed. Numerical simulations of crash tests for both steel and composite crash boxes are performed to obtain energy absorption values derived from load-displacement data. In order to compare specific energy absorption capacity and estimate the optimum thickness of composite crash box, same geometry with steel is also modelled in ABAQUS/Explicit. The cross- sectional view of the sandwich structure with dimensions is given in Figure 4.4.

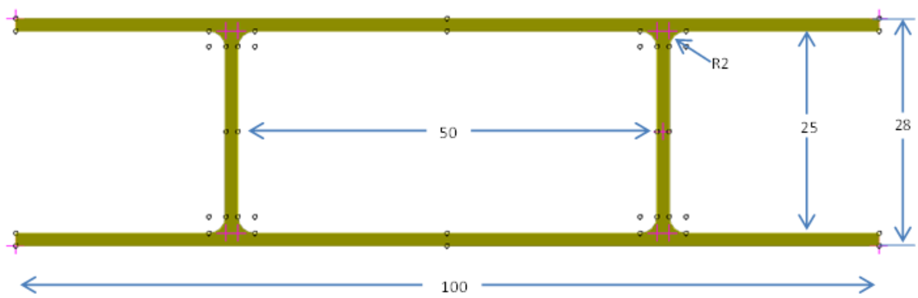

Figure 4.4. Cross-sectional view of sandwich structure (All dimensions are given in mm.)

4.3.1. Numerical Analysis of Metal Specimen

The finite element model includes a deformable model of the crash-box. The 3D drawing of the sandwich crash box is given in Figure 4.5. Material used in the analysis is DP600 Steel with the density value of 7.85 g/cm^3, elastic modulus of 210 GPa and the Poisson's ratio of 0.3 [40].

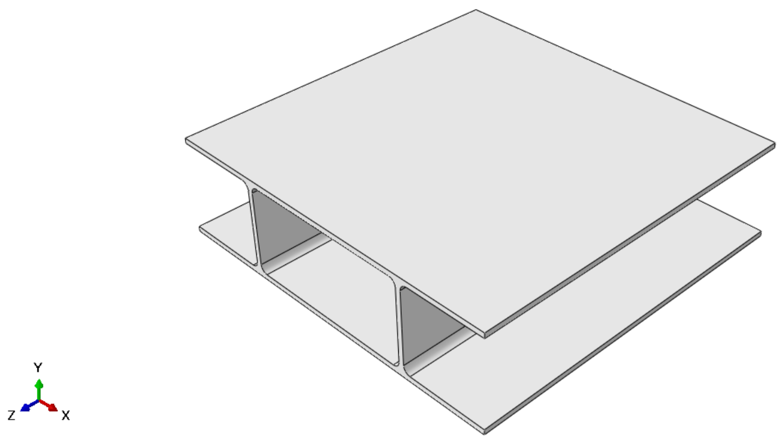

Figure 4.5. The 3-Dimensional view of the metal specimen

Metals show an increase in their yield strength with an increase in plastic strain as well as strain rate. During a crash, the boxes severely deform in a very short time. That is why a realistic simulation of a crash event requires a constitutive equation that accounts for non-linear and strain-rate dependent deformation. In the present FE model, Strain-rate dependent tabular data [40] is used (see Figure 4.6).

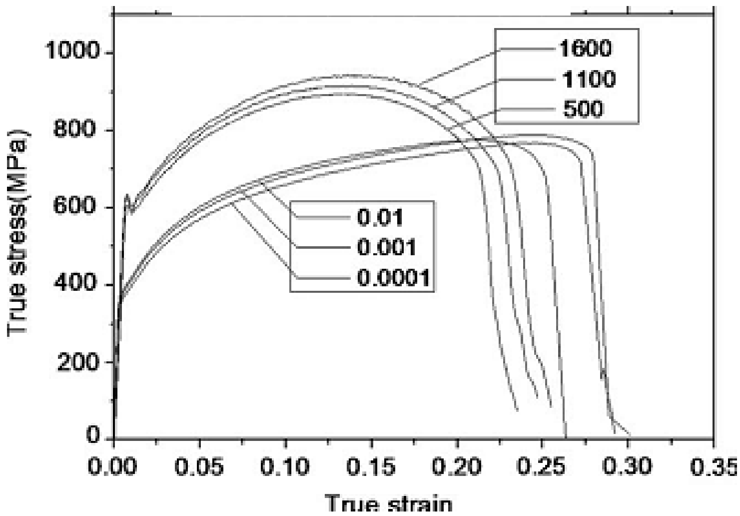

Figure 4.6. True stress- strain curves of DP600 Steel at six different strain rates [s^{-1}] [40]

As in other analyses, steel specimen is placed between the two rigid plates. For applying initial and boundary conditions, upper rigid wall (the impacter) has an initial velocity of 300 mm/s. All degrees of freedom in the lower plate and all degrees of freedom in the upper plate, except in the direction of crushing (z) axis, were constrained. Crash box is built as solid elements while shell elements are used in rigid impacter.

4.3.2. Numerical Analysis of Composite Specimen

The benchmark model defined in section 4.2 was studied to elucidate the progressive crush failure model in ABAQUS consisting in-plane and delamination damages. In this section, comprehended and validated model is applied to a composite sandwich structure with a different material, namely AS4/8552, which is a carbon/epoxy prepreg supplied by Hexcel.

Finite element model of a carbon–epoxy composite specimen with the novel geometry is simulated in ABAQUS/Explicit. The specimen, in which $[0/90]_{2S}$ composite lay-up used, is 1.5 mm thick and 100 mm long. Because the geometry of the crash-box and the loading are symmetric with respect to the horizontal and vertical mid-planes, only one quarter of the assembly is analysed and the necessary symmetry conditions are applied on the corresponding interfaces. Figure 4.7 shows the quarter model. Since the crushing behaviour is simulated in two-dimensional model, the extrusion of the bead is changed as illustrated in Figure 4.8. By doing this, the intralaminar and interlaminar behaviour of the bead can be simulated.

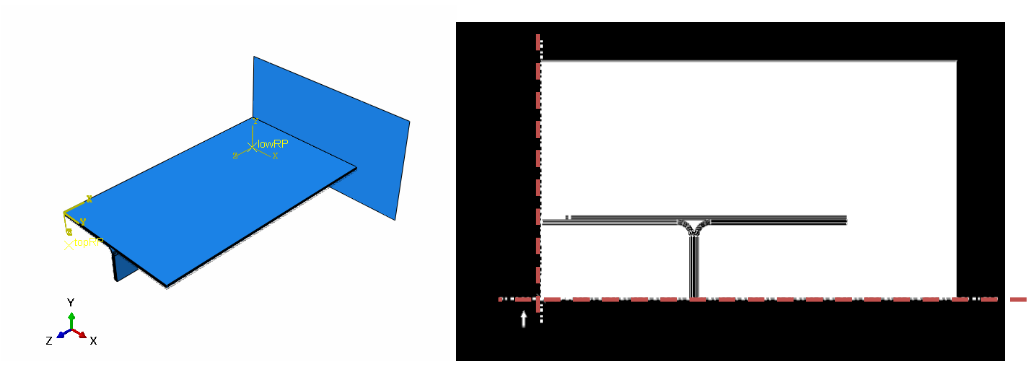

Figure 4.7. a) Quarter model of the composite sandwich structure b) front view with symmetry axes

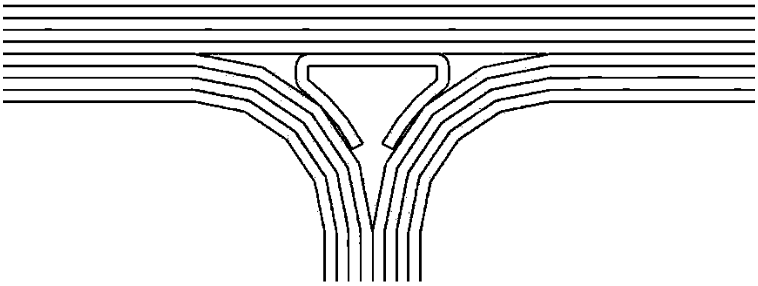

Figure 4.8. Illustration of the bead in the assembly.

The material used for this model is AS4/8552 carbon-epoxy. Table 4.3 shows the material properties. For interlaminar properties to apply cohesive zone modelling, all of the required data is not available in the literature. At that point, fracture toughness data for a very similar carbon fibre/epoxy (IM7/8552) is taken from the study of Hallett et al. [41]. The properties used for cohesive zone model is given in Table 4.4.

Table 4.3. Material properties of AS4/8552 composite

Description	Variable	Value
Density [g/cm3]	ρ	1.58
Longitudinal modulus [GPa]	E_{11}	141
Transverse modulus [GPa]	$E_{22}=E_{33}$	97.55
Principal Poisson's Ratio	v_{12}	0.267
Shear Moduli in 1-2 plane [GPa]	$G_{12}=G_{13}$	5.2
Shear Moduli in 2-3 plane [GPa]	G_{23}	3.19
Longitudinal Tensile Strength [MPa]	X_{1+}	2200
Longitudinal Compressive Strength [MPa]	X_{1-}	1500
Transverse Tensile Strength [MPa]	Y_{2+}	81
Transverse Compressive Strength [MPa]	Y_{2-}	260
In-plane Shear Strength [MPa]	S	80

Element type and boundary conditions are applied as described in the benchmark study. The velocity of the impacter is chosen as used in the simulation of metal specimen, which is 300 mm/s. The analysis consists of a single explicit dynamic step. In the simulations, automatic time incrementation is used with element-by-element stable time increment estimates.

Table 4.4. Interlaminar properties of IM7/8552 composite

σ_{33c} (MPa)	σ_{13c} (MPa)	σ_{23c} (MPa)	G_I^c(J/mm^2)	G_{II}^c(J/mm^2)	G_{III}^c(J/mm^2)
54	70	70	0.2	0.8	0.8

In Section 4, four different numerical analyses are taken into consideration that contains the models of delamination, benchmark study and sandwich crash box structures with metal and composite materials. Results are discussed in Section 6 in detail. At the end of all analyses, in order to present a clear definition, details related to FEA developed for the progressive crushing process of composite crash box are listed in the following steps;

1. Creation of parts of the model as three dimensional extrusions. Each ply is extruded separately.
2. Material properties definition and assignment.
3. Material failure criteria definition.
4. Composite lay-up assignment in which continuum shell elements are selected.
5. Orientation indication.
6. Assembly of all single parts.
7. Interaction properties assignment. Cohesive surfaces are identified separately with the assigned properties.

8. Mesh creation with continuum shell elements and stack direction assignment.

9. Definition of the boundary conditions and load.

10. Job creation.

5. EXPERIMENTAL STUDY

In the experimental part of this study, a quasi-static compression test is carried out on CRFP sandwich structure. The main objective of the experiment is to visualize the behaviour of the composite material under quasi-static compressive loading and to obtain load-displacement curve for verification with the numerical results. The material and stacking is chosen as $[0/90]_{2s}$ which are the same with the properties in the model of corrugated specimen.

5.1. Specimen Preparation

The sandwich structure is manufactured from Hexcel AS4/8552 carbon-epoxy unidirectional prepregs. Manufacturing process is carried out in an autoclave with a depth of 1500 mm and inner diameter of 1200 mm. An autoclave is a kind of pressure vessel in which temperature and pressure can be controlled. In the autoclave manufacturing technique, prepregs are stacked on the mould by hand lay-up technique. The schematic representation of the lay-up method is given in Figure 5.1. Prepared laminate is vacuumed in a vacuum bag and heated as demonstrated in Manufacturer Recommended Cure Cycle (MRCC). With the help of pressure, voids in resin are minimized. During the curing process, resin is hardened or toughened by crosslinking of polymer chains. In addition, resin and fibre are bonded chemically. MRCC for AS4/8552 prepreg produced by Hexcel could be seen in Figure 5.2.

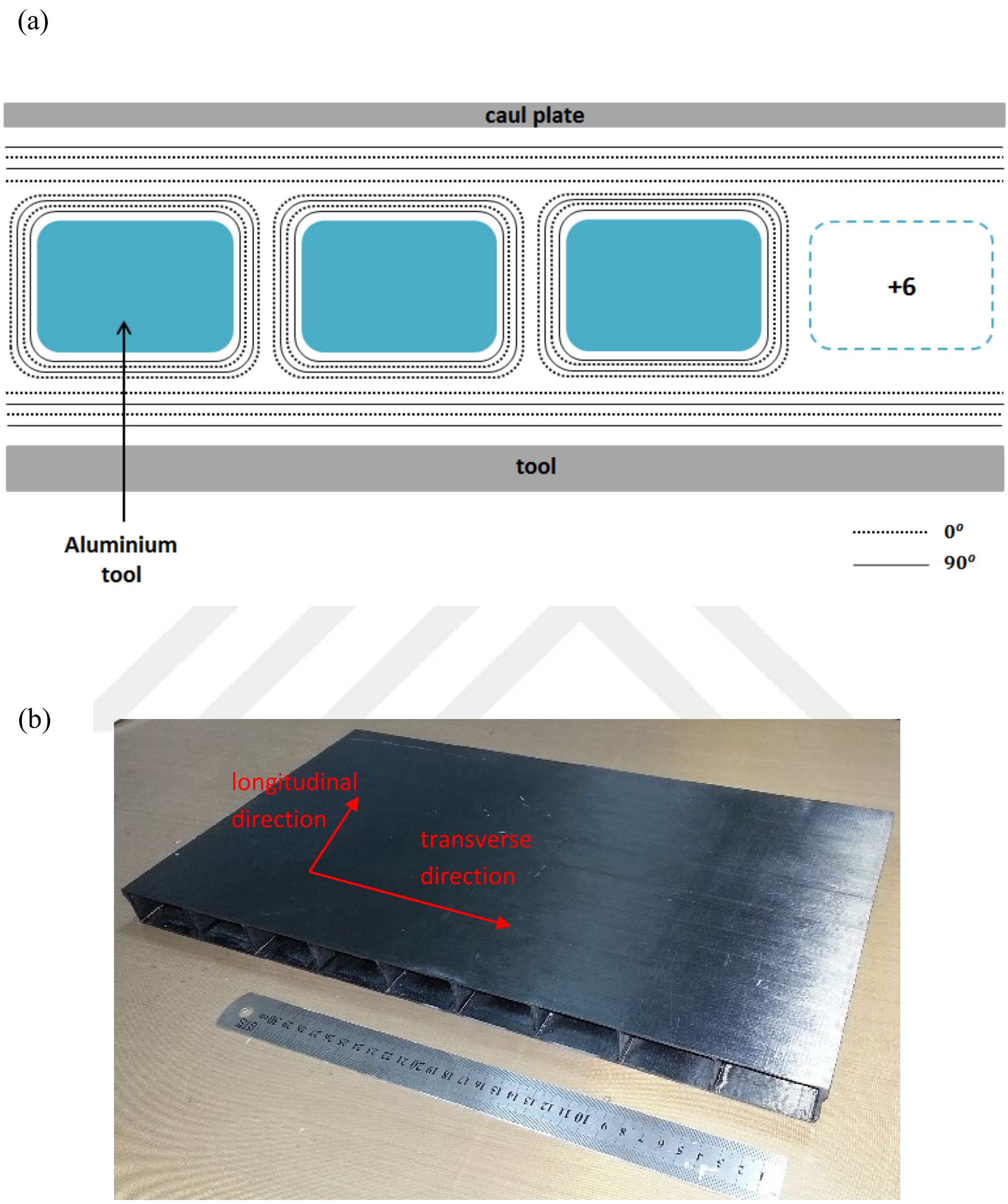

Figure 5.1. (a) Schematic representation of the lay-up method. (b) Manufactured sandwich panel.

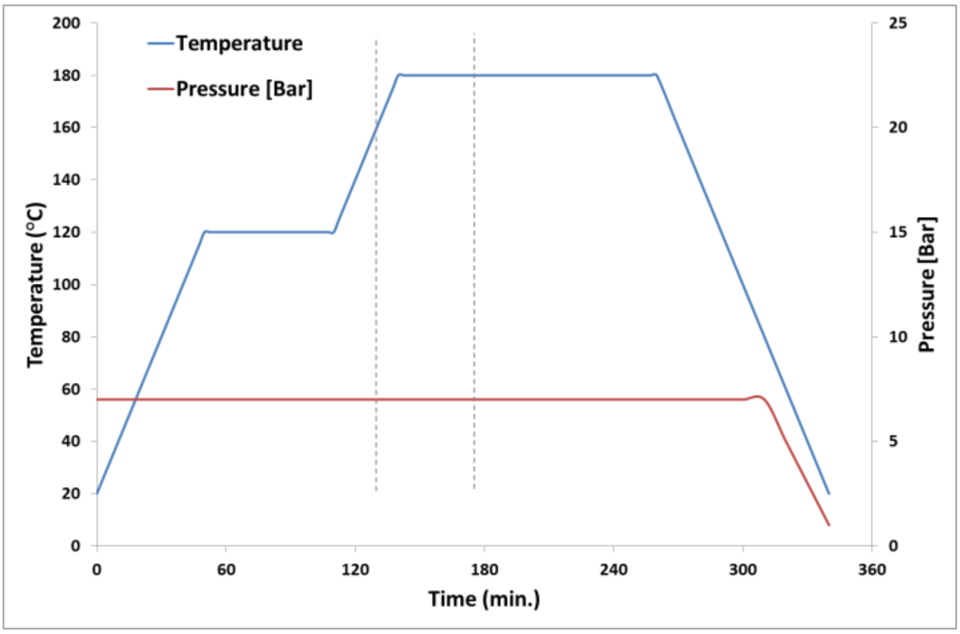

Figure 5.2. Manufacturer Recomended Cure Cycle in terms of temperature and pressure

The sandwich panel shown in Figure 19b is then cut by a diamond cutter into 100 mm X 100 mm parts with 1.5 mm thickness. The compression surfaces is machined to guarantee to be parallel to each other and chamfered in a milling machine. The final weight of the specimen is 56.51 grams. Close-up photo of a finalized specimen is presented in Figure 5.3.

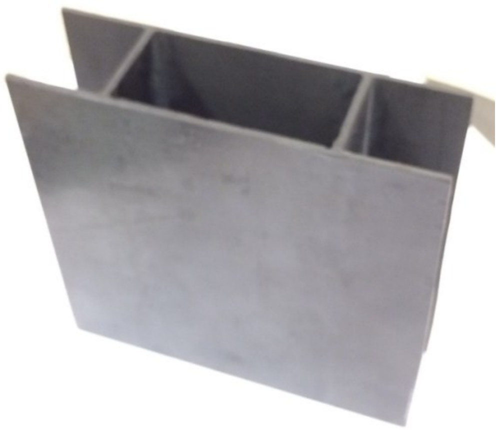

Figure 5.3. Test Specimen for the novel geometry

5.2. Test Procedure

The specimen is tested in the vertical configuration standing free on the steel surface of the Instron Universal Testing Machine (Model 3369). The upper plate of the experimental rig was moving downwards during the experiments. A self-aligning sphere joint was used to introduce the crushing load from the test frame onto the specimen. Because the corrugated specimen is self-supporting, no supports were used on the specimens. The testing was performed at a quasi-static speed of 0.5 mm/min. Fig. 5.4 shows the experimental setup.

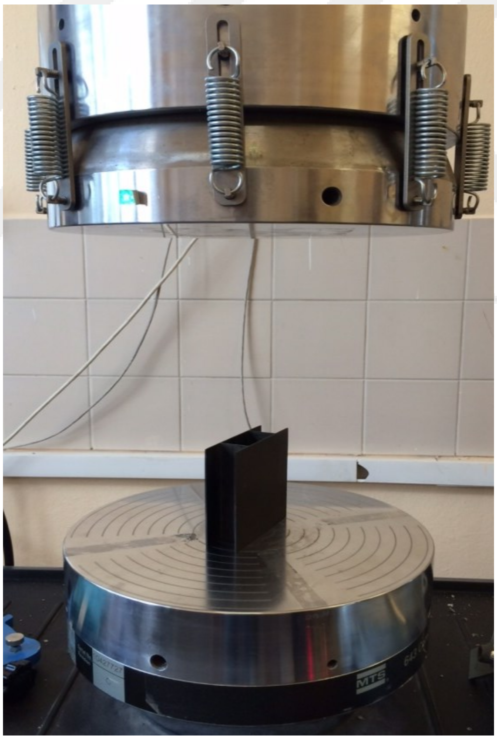

Figure 5.4. Experimental Setup

6. RESULTS AND DISCUSSION

The main purpose of the thesis was to develop a numerical model for crushing process of composites. Progressive failure during crush consists of interlaminar and intralaminar progressive failure. For the interlaminar failure analysis, a methodology for predicting accurately the propagation of delamination under mixed-mode fracture with cohesive elements was proposed. At that point, simulation of the delamination behaviour of the two dimensional simple composite geometry is used for validation. Results will be given in section 6.1.

Moreover, modelling of the crushing process of composite crash box for a specific geometry existing in the literature was also studied for benchmarking purposes. A finite element model, which includes the intralaminar and interlaminar progressive failure analysis of composite crash box, was developed. First, in order to discuss the accuracy of the developed numerical method, results obtained from FE analysis and taken from the original study will be compared in this section.

Additionally, this thesis work also presents the numerical analysis of the composite crash box with a novel geometry. AS4/8552 carbon-epoxy material was selected as a model material for that crash box because of the availability of the material itself as well as the material property database. Although the intralaminar material properties were found from the experimental studies in literature, the required data for interlaminar properties of the material couldn’t have been reached. Therefore, the interlaminar properties of a similar material, namely T700/8552 were used in model since the matrix is the same, and the interlaminar properties are mostly resin-dominated. For validation, composite crash box was manufactured in order to observe crushing behaviour experimentally. With the help of the experimental measurements, load results of the FE method with the estimated interlaminar properties can be validated.

Finally, in order to compare the energy absorbing capacities, numerical analysis of DP600 Steel crash box was also done. By comparing the absorbed energy values between the metal and composite specimens, the optimality of the thickness of composite crash box can be discussed.

6.1. Results of Basic Delamination Model

As one of the significant part of the thesis, Cohesive Zone Model (CZM) approach, suitable for modelling delamination propagation, was adopted. Decohesion elements use failure criteria that combine aspects of strength-based analysis to predict the onset of the softening process at the interface between laminae, and Fracture Mechanics to predict delamination propagation. Details about model were given in Section 3.2. The model was validated by simulating the delamination behaviour of the two dimensional simple composite geometry with eight plies. The results for delamination growth are shown in Figure 6.1.

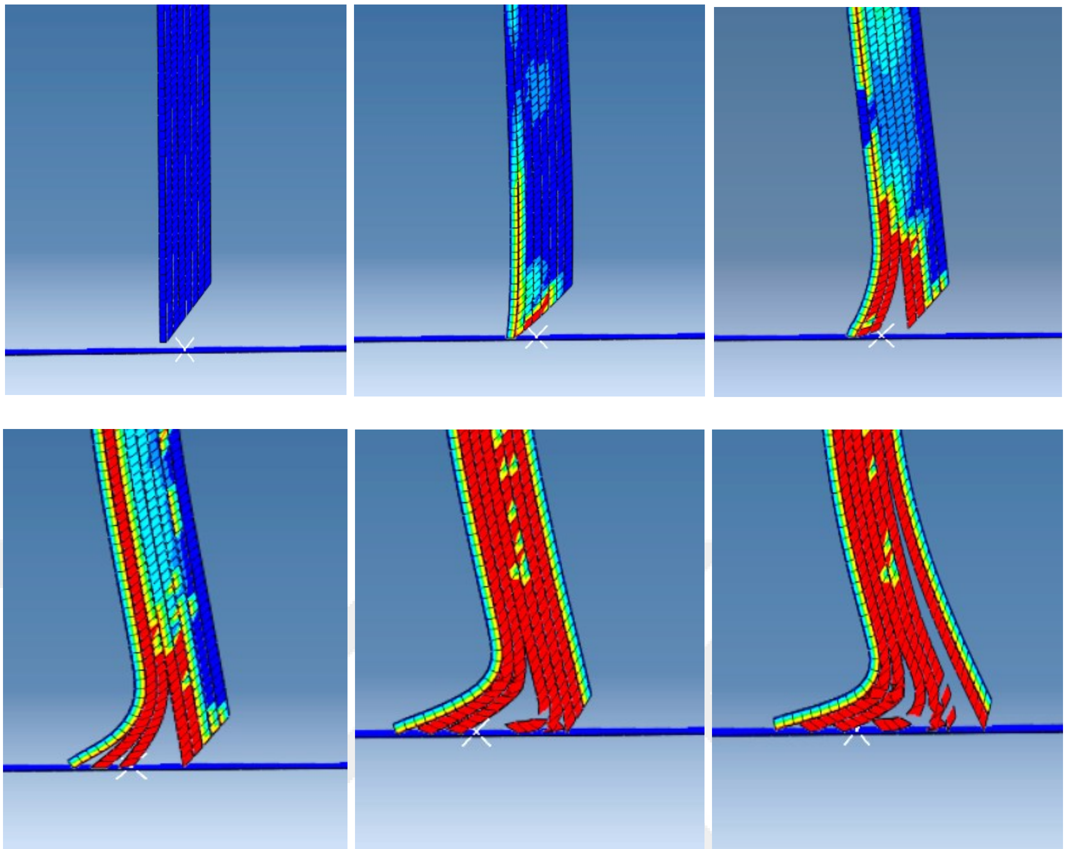

Figure 6.1. Delamination growth of the 2D specimen

As mentioned, the analysis was carried out to study the effect of the CZM. Numerical simulation showed that the model developed in ABAQUS is able to model the smooth, progressive delamination. As an advantage, CZM can be effectively used in a range of different element sizes and can save a large amount of computation. According to Figure 6.1, the capability of the model is proved by the reasonable delamination growth. Furthermore, results show the significance of 45^{o} chamfer as delamination initiator. Chamfer behaves as trigger and avoids buckling and higher initial load peak which would lead to destruction of other structural parts.

6.2. Results of Benchmark Study

The deformed shape of the sinusoidal shaped plate at crushing simulation is shown in Figure 6.2. Note that the deletion of damaged elements in the plies creates detached parts that are removed from the model as explained previously. It can be seen from the deformation results that the ABAQUS/Explicit simulation reproduced important characteristic features of the crushing response of composites. Moreover, a close match between the published study (Sokolinsky et al. [19]) and simulated load displacement curves is demonstrated in Figure 6.3. According to these results, it can be said that both the peak and average crush forces were predicted reasonably well.

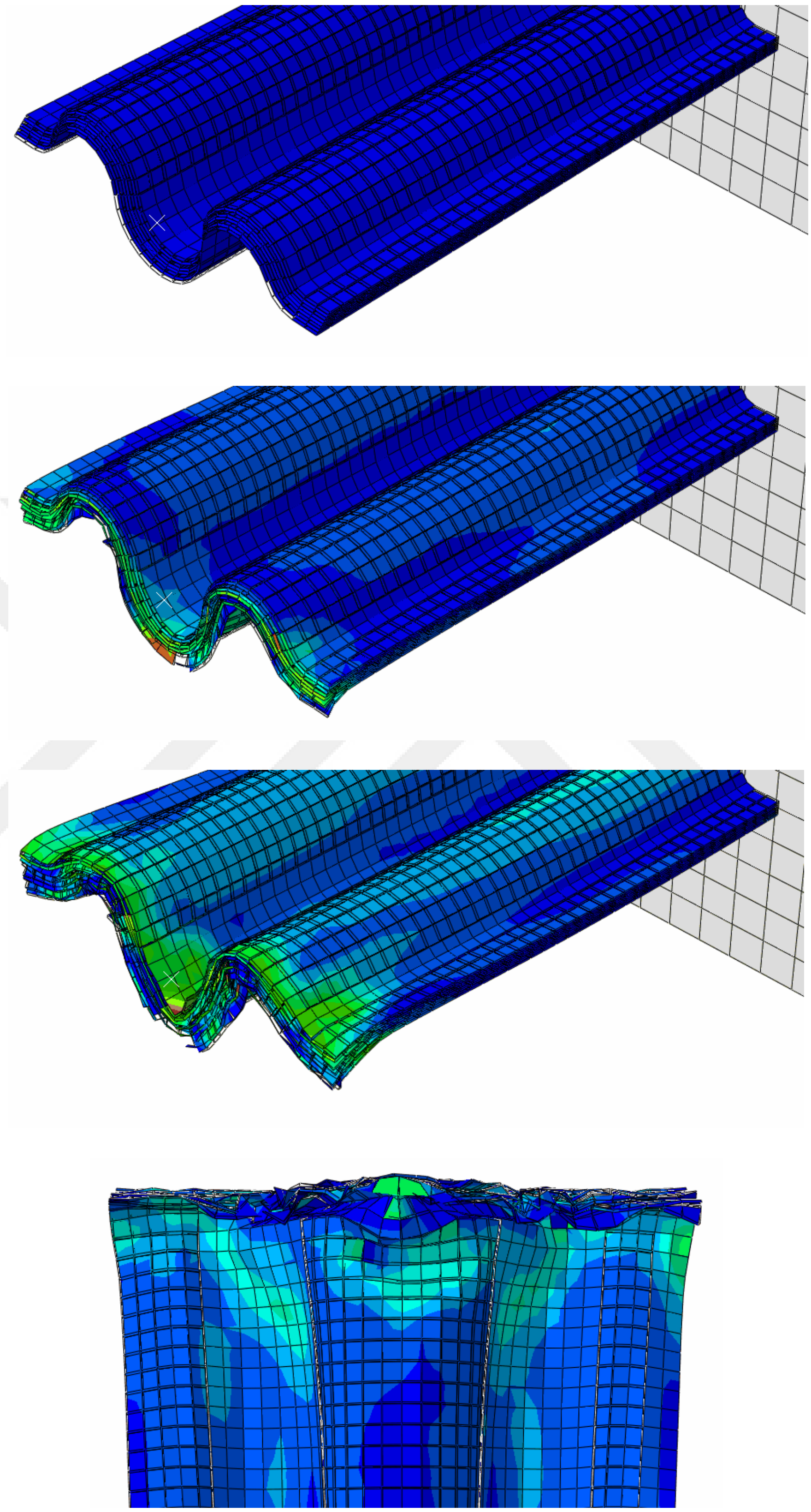

Figure 6.2. Crushing Process of the plate

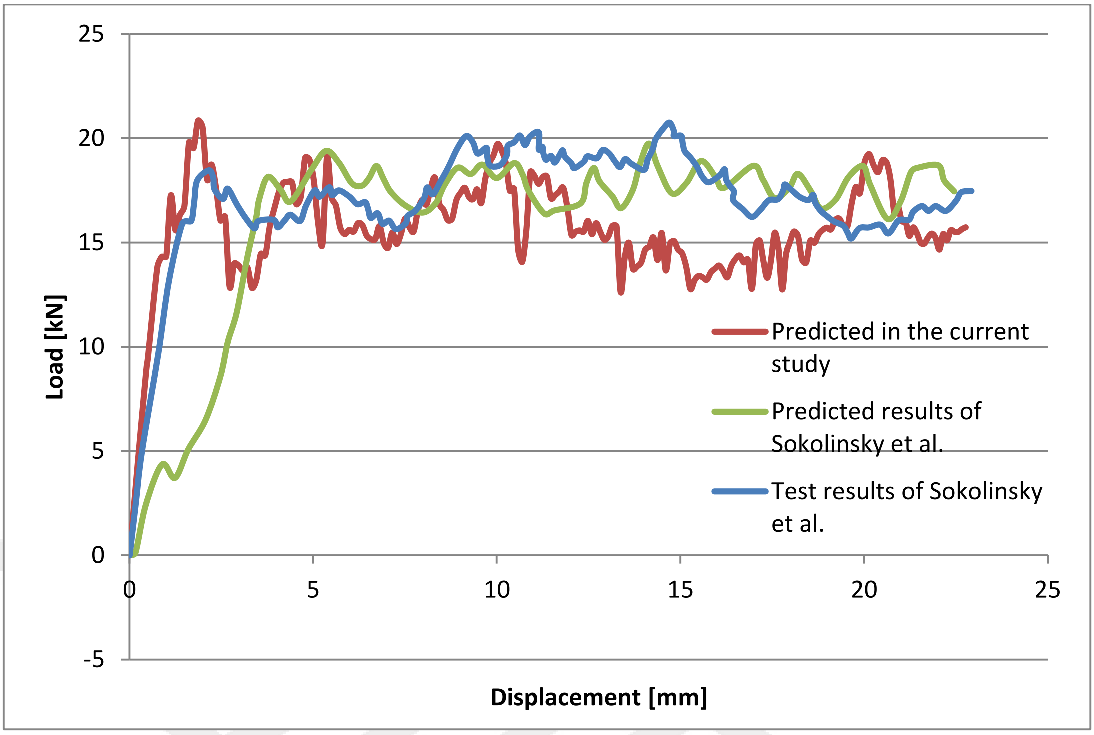

Figure 6.3. Comparison between the load–displacement curves of the published study [19] and predicted numerically in this study.

The numerical results for the energy absorbed versus stroke, which is calculated as the total area under the load–displacement curve in Figure 6.3, are shown in Figure 6.4. The term stroke is the length of the plate that has been destroyed during crushing. As can be seen from the figure, the original and numerically predicted curves nearly coincide with each other.

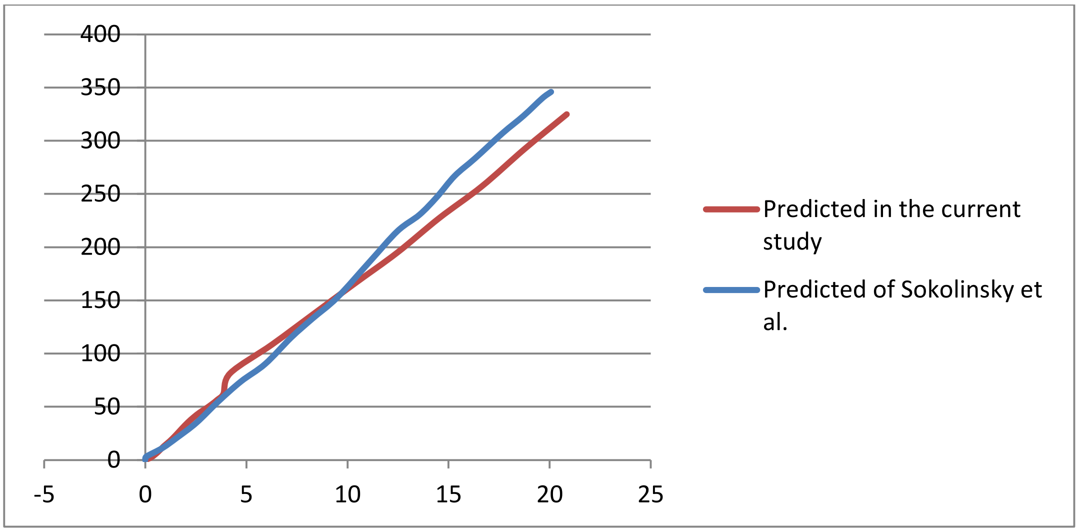

Figure 6.4. A comparison between the absorbed energy values in the published study [19] and predicted numerically in this study

Finally, a comparison between the experimental and simulated specific energy absorption (SEA) of the novel crash box based on sandwich plate is done. SEA shows the ability of a material to dissipate energy; it is measured in Joules per gram and computed by dividing absorbed energy by the crushed mass of the plate, which can be expressed as the product of the stroke, cross-sectional area of the plate, and its density. From the study of Sokolinsky et al., the specific energy absorption value is 85 J/g when the material is crushed for 20 mm. This value is 86.062 J/g evaluated from the numerical analysis in this study. Taking into consideration the extremely complicated nature of the crushing process, the overall correspondence between the original and simulated SEA results can be said to be very well.

As a result, it can be deduced that the benchmarking study of Sokolinsky's work is achieved successfully and the accurate model with intralaminar and interlaminar damage mechanisms, which can be applied for other geometries, was developed.

6.3. Results of the Sandwich Structure

According to the model that simulates crushing process of the composite crash box with a sandwich structure, the deformation of the specimen is shown in Figure 6.5. According to results, it can be said that brittle fracturing crushing mode was observed which is a combination of fragmentation and splaying crushing modes. As previously indicated, the experimental study was also carried out for comparison with numerical simulation. Figure 6.7 demonstrates the crushed composite structure at the end of the quasi-static compression test. Please note that the model is only a quarter of the structure since the symmetric nature of the structure is taken into account.

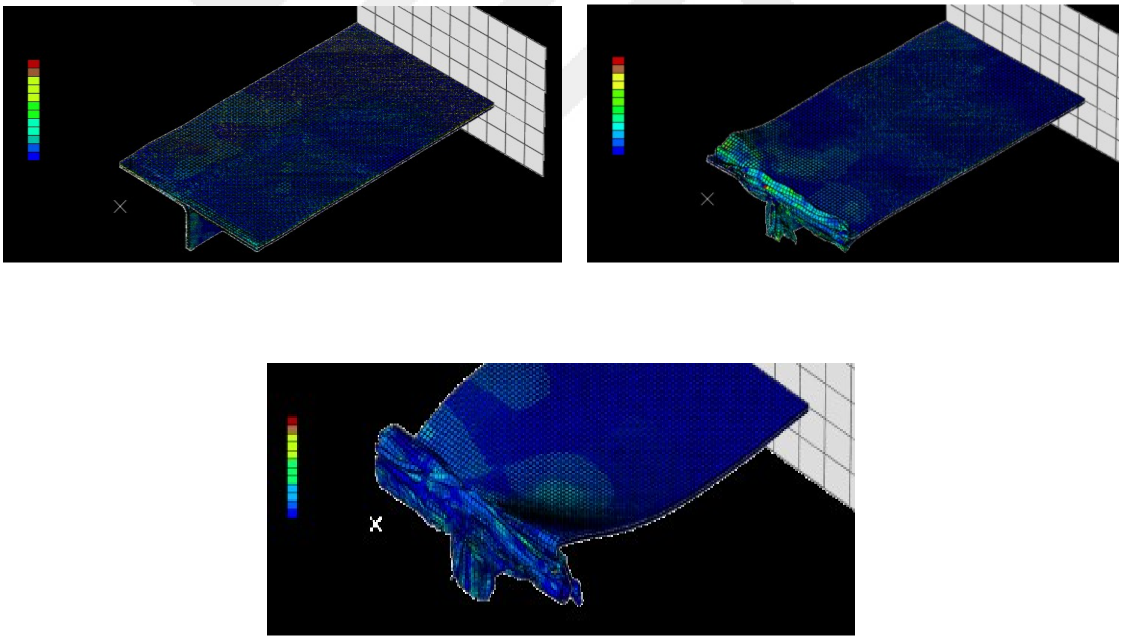

Figure 6.5. The deformation of the composite crash box with sandwich structure (quarter model).

The simulation time was one of the challenges for modelling in ABAQUS. Instead of solid elements, continuum shell elements were used and element size is increased to reduce the simulation time. Moreover, mass scaling was employed in order to achieve a reasonable run time.

The other challenge for this numerical analysis was the occurrence of excessive distortion errors during simulation. The excessive deformation of a three-dimensional element under axial loading (see Figure 6.6) makes the running simulation aborted at the beginning of the analysis. Mass scaling was one of the recommended solutions to overcome this problem; so it is applied. In addition, the velocity is reduced and step time is increased. Different mesh sizes were applied and the damage variable criterion for element deletion is also reduced in order to delete elements before excessively distorted. In the final model, a uniform mesh with an element size of 1 mm by 1 mm was used for each ply. When simulation time is taken into account, mesh convergence study couldn't have been applied. Element size is indicated as the minimum value that does not cause excessive distortion. As a result, the model, with 56800 elements and 0.01 seconds step time period, required approximately one week of running time on 8-Core computer.

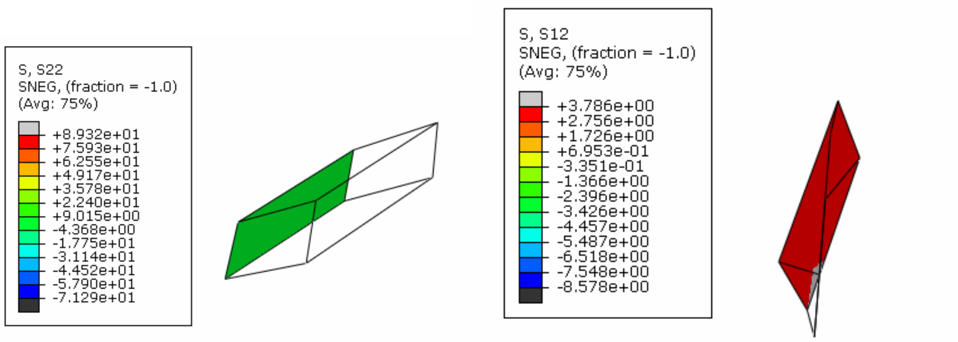

Figure 6.6. Distorted element at crash simulation. a) at the beginning, b) after element is distorted.

At the end of the quasi-static compression test, corrugated specimen is crushed as shown in Figure 6.7. The load-displacement output of the numerical analysis is given in Figure 6.8 together with the experimental results.

Figure 6.7. Crushed corrugated specimen at the end of the compression test.

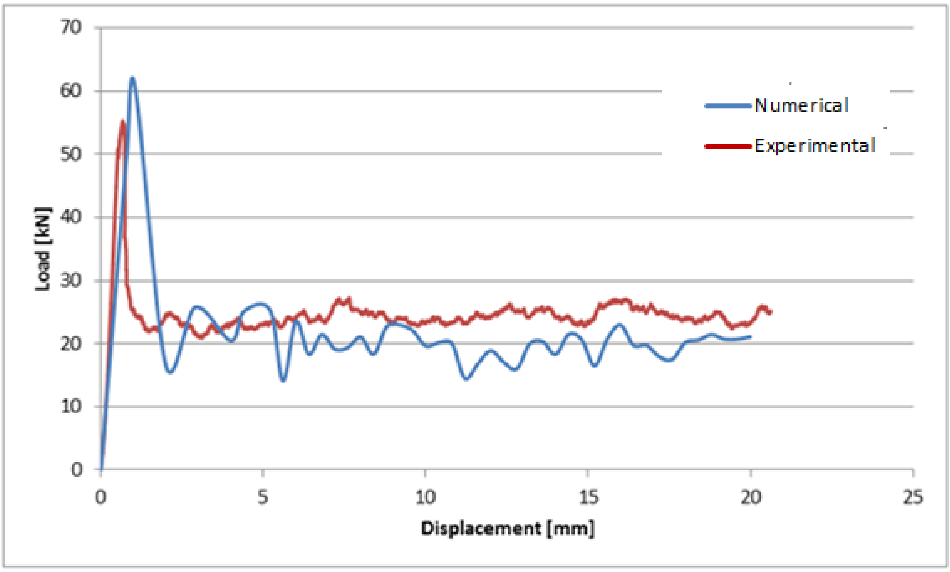

Figure 6.8. Comparison of the experimental and numerical load–displacement curves of corrugated crash box.

As can be seen from Figure 6.8, the specimen was crashed by 20 mm. When, both the peak and average crush forces are compared, the difference between two curves is not too much. It should be noted that by measuring actual interlaminar properties, better accuracy can be obtained. However, when challenges and simulation time are taken into consideration, the accuracy of the results is accepted as quite reasonable. By calculating the total area under the load-displacement curve, the numerical and experimental results for the absorbed energy is obtained as shown in Figure 6.9. At the point that the crushed length reached to 20 mm, the numerically obtained value of energy absorbed by the crash box is 435.6 J. According to this result, it can be said that novel geometry absorbed more energy than the sinusoidal geometry of the benchmark study. The specific energy absorption value of the novel geometry is 44.59 J/g in average.

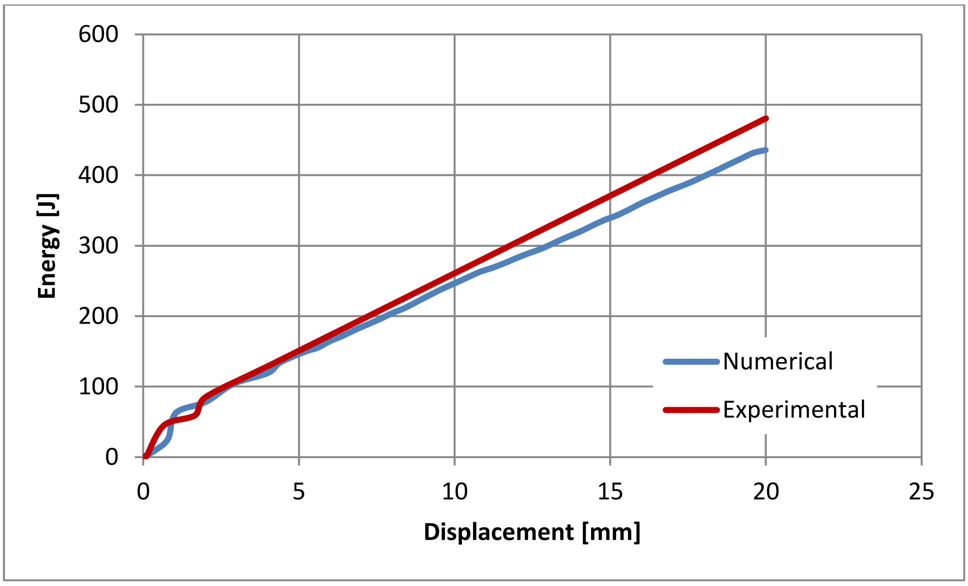

Figure 6.9. Numerical and experimental results for the absorbed energy for composite sandwich crash box

In order to compare the composite and the metal structures, the numerical analysis of metal crash box was done for the same geometry and the load-displacement curves and absorbed energy values of the metal and composite structures are compared in Figures 6.10 and 6.11. According to overall comparison given in Table 6.1, it is hard to say that composite crash box can substitute a metal crash box while both having same thicknesses. The amount of energy absorbed for metal crash box at 20 mm crushed length is 1654.6 Jules which is approximately four times higher than the energy absorbed by the composite structure. On the other hand, recent composite crash box is %88 lighter than the metal one. If the specific energy absorbing capacities (SEA) are compared, composite crash box has 2.4 times higher SEA. In order to reach an optimum design for higher absorbed energy, the thickness and the weight of composite crash box can be increased.

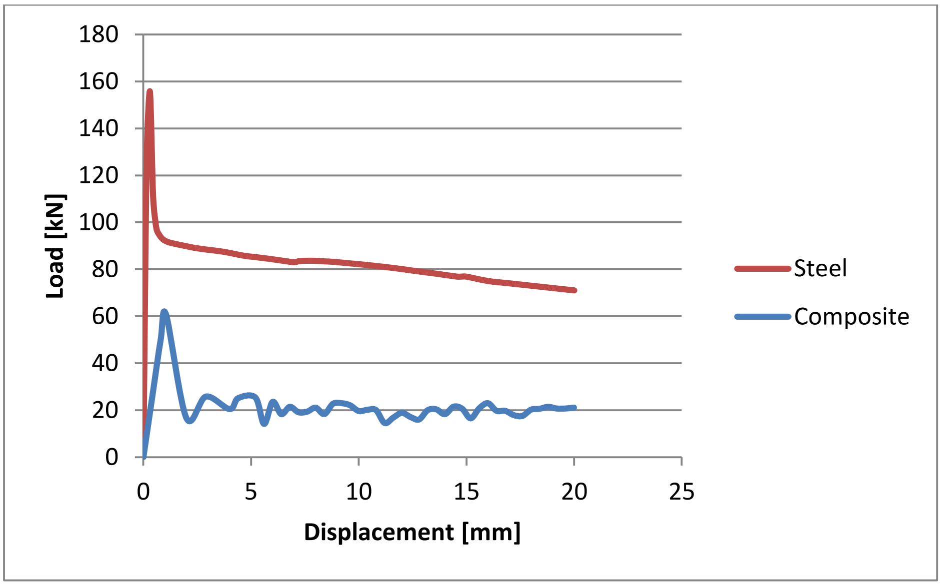

Figure 6.10. Load-displacement curve of the steel and composite crash box

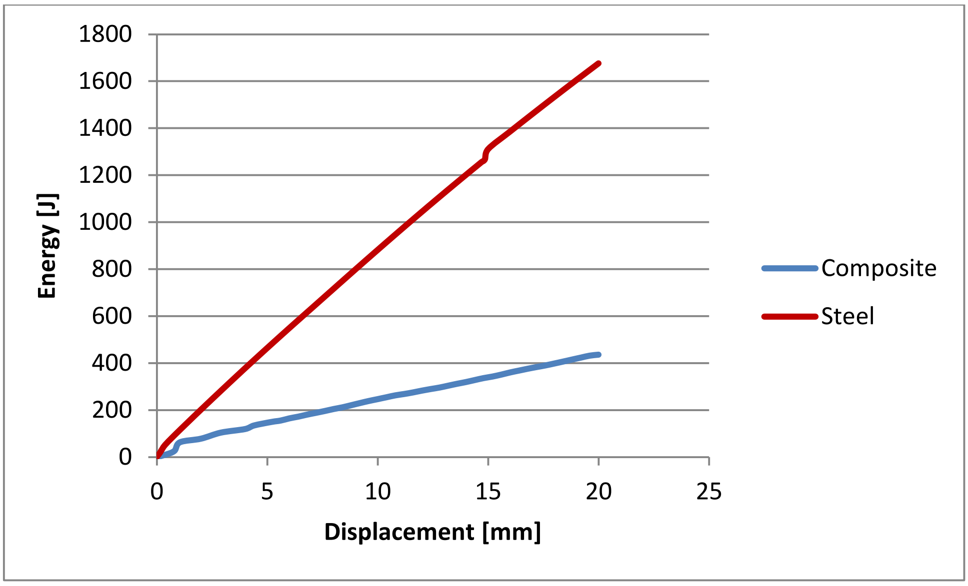

Figure 6.11. Numerical absorbed energy results of composite and steel crash boxes.

Table 6.1. Comparison of energy absorption values between composite and metal crash boxes

Crash Box Material	Thickness [mm]	Weight [g]	SEA [J/g]	Energy absorbed for 20 mm crush [J]
Composite	1.5	52.8	44.59	435.6
Metal	1.5	448	18.47	1654.6

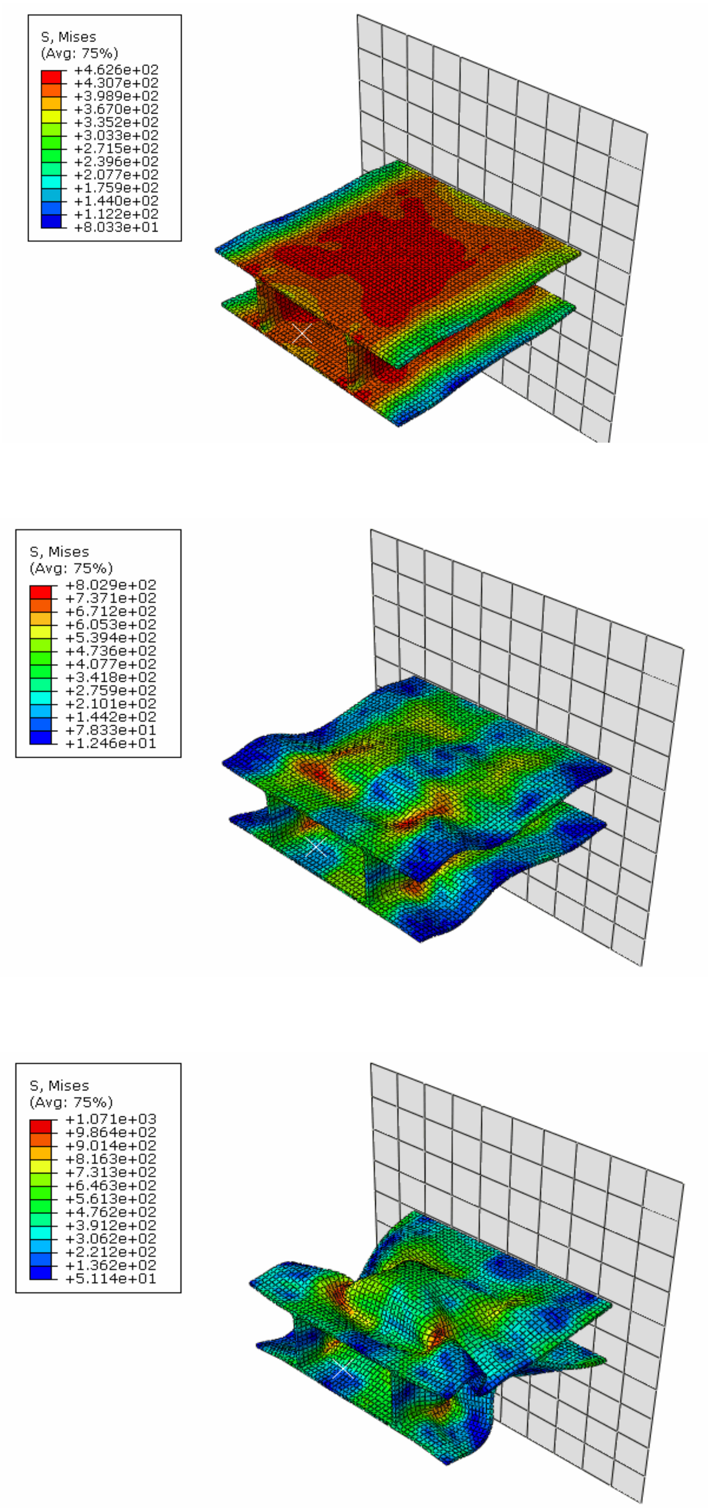

Figure 6.12. Deformed shape of the metal crash box

7. CONCLUSIONS AND FUTURE WORK

In this study, modelling of the crushing process of composite crash box for a specific geometry existing in the literature was studied for benchmarking purposes. A finite element model of progressive failure analysis of composite crash box, including intralaminar failure and delamination behaviour, was developed in ABAQUS/Explicit. For damage initiation, Hashin damage criteria, which is default in ABAQUS, was applied. Moreover, CZM was used to simulate the delamination process. The comparison between the model predictions and published results showed that the model can predict the energy absorption of the crash box very accurately.

After benchmarking study, validated ABAQUS/Explicit finite element code was used to simulate the behaviour of composite crash box with a novel geometry (sandwich structure). AS4/8552 carbon-epoxy material was selected as a model material because of the availability of the material itself as well as the material property database. For the interlaminar properties, data of a similar material, namely T700/8552 were used in model. By determining the crash performance of the sandwich structure experimentally, numerical and experimental results were compared and interlaminar properties were validated. Consequently, the numerical results pertaining to the load-displacement curve as well as energy absorbing capacity of the sandwich structure are close to the experimentally measured values with an acceptable accuracy.

Finally, numerical analysis of DP600 Steel crash box having same geometry with the sandwich composite structure was applied to compare the energy absorbing capacities and discuss the optimality of the composite design. According to comparison, although the specific energy absorption value of composite is higher than metal crash box, the absorbed energy results of the composite structure fell behind the metal crash box. That is why; composite crash box with selected thickness value cannot be utilized as the substitution of metal version. At that point, as a future work, a new thickness and lay-up design for same geometry, as well as other geometry options can be implemented to find an optimum crash box that absorbs more energy with less weight than the metal design. On the other hand, future research can include a further validation of the numerical model with other damage criteria and for different geometries and materials.

REFERENCES

1. "AUTOMOTIVE COMPOSITES DRIVING THE CHANGE Thermoplastic and thermoset composites for automotive applications," TENCATE Catalogue, http://www.tencate.com/emea/Images/TCAC_DrivingTheChange_V1_021914_Web_tcm28-28531.pdf, June 2016.

2. "Kompozitler Dünyası ve Otomotiv," *Composites Turkey*, Eylül 2014, Sayı: 8, 28-37.

3. "Traffic Safety Facts-Research Note," US Department of Transportation, National Highway Traffic Safety Administration, February 2012.

4. Ghassemieh E., "Materials in Automotive Application, State of Art and Prospects" in *New Trends and Developments in Automotive Industry*, Edited by Chiaberge M., www.intechopen.com, 2011.

5. Tanlak N., F. O.Sonmez, M. Senaltun, "Shape optimization of bumper beams under high-velocity impact loads", *Engineering Structures,* no. 95, pp. 49–60, 2015.

6. Vıllalonga R., Th.Enderich, "Advanced Simulation Techniques for Low Speed Vehicle Impacts", *LS-DYNA Anwenderforum*, Frankethal, 2007.

7. Shen Z., X.Qiao, H. Chen, "BIW Safety Performance Research Based on Vehicle Frontal Crash", *Proceedings of the FISITA 2012 World Automotive Congress Volume 9: Automotive Safety Technology*, Eds. SAE-China, FISITA, 2013

8. Brown J. S. "Design Optimization of Front Bumper System for Low Speed Impact Insurance Industry Impact Test using DFSS and CAE Analysis", *SAE International Journal of Passenger Cars - Electronic and Electrical Systems*, Vol.4, No. 1, pp.62-68, June 2011

9. Yin H., G.Wen, H.Fang, Q.Qing, X.Kong, J.Xiao, and Z. Liu, "Multiobjective crashworthiness optimization design of functionally graded foam-filled tapered tube based on dynamic ensemble metamodel", *Materials & Design*, Vol. 55, pp. 747–757, March 2014

10. Houssini S. E. “Front Bumper Crashworthiness Optimization”, *Proceedings of the 9th International LS-DYNA Users Conference*, Dearborn, Michigan, 2006.

11. Öztürk İ., Kaya N., “OTOMOBİL ÖN TAMPON ÇARPIŞMA ANALİZİ VE OPTİMİZASYONU”, *Uludağ Üniversitesi Mühendislik-Mimarlık Fakültesi Dergisi*, Cilt 13, Sayı 1, 2008.

12. Ghasemnejad H., H. Hadavinia, A. Aboutorabi, “Investigation of energy absorption of a GRFP composite crash box”, *Structures under Shock and Impact X*, Proceedings of SUSI 2016: 14th International Conference on Structures under Shock and Impact, 24 - 26 May 2016 Crete, Greece, Edited By: N. JONES, University of Liverpool, UK and C.A. Brebbia, Wessex Institute of Technology, UK,

13. Hull D. “Energy absorption of composite materials under crash displacement variables obviates the need for special element types that are not available in crash codes”, in: *Proceeding of the 4th International Conference on Composite Materials: Progress in Science and Engineering of Composites,* held in Tokyo, Japan, pp. 861–87. 1982.

14. Farley G.L. “Energy absorption of composite materials”, *Journal of Composite Materials*, Vol. 17, No. 3, pp. 267-279, 1983.

15. Mamalis A.G, Manolakos D.E., Ioannidis M.B., Kostazos P.K., Papapostolou D.P. “Axial collapse of hybrid square sandwich composite tubular components with corrugated core: numerical modelling” *Composite Structures*, 58, pp. 571-582, 2009.

16. Hörmann M., Wacker M. “Simulation of the Crash Performance of Crash boxes based on Advanced Thermoplastic Composite” *5th European LS-DYNA Users Conference.*

17. El-Hagel H., Mallick P.K., Zamani N. “Numerical modelling of quasi-static axial crash of square aluminum-composite hybrid tubes”, *International Journal of Crashworthiness,* No. 9, pp. 653–64, 2004.

18. Indermuehle K., Barnes G., Nixon S., Schrank M. “Simulating Composites Crush and Crash Events Using Abaqus” *50th AIAA/ASME/ASCE/AHS/ASC Structures, Structural Dynamics, and Materials Conference*, 2009

19. Sokolinsky V.S., Indermuehle K., Hurtado, J. A., “Numerical simulation of the crushing process of a corrugated composite plate”, *Composites*, Part A, No. 42, pp. 1119–1126, 2011.

20. A Safety Roadmap for Future Plastics and Composites Intensive Vehicles, *National Highway Traffic Safety Administration*, Report No: DOT HS 810 863, 2007.

21. Kleisner V., Zemcık A., “Analysis of composite car bumper reinforcement” *Applied and Computational Mechanics*, No. 3, pp. 287–296, 2009.

22. Pinho S.T., Davila C.G., Camanho P.P., Iannucci L., Robinson P., “Failure models and criteria for FRP under in-plane or three-dimensional stress states including shear non-linearity”, NASA/TM-2005-213530, 2005.

23. Hyer M. W., *Stress Analysis of Fibre-Reinforced Composite Materials,* McGraw-HILL INTERNATIONAL EDITIONS, 1997.

24. Andersen M., Liedberg P., *Crash behaviour of composite structures, A CAE benchmarking study*, Master's thesis, Chalmers University of Technology, 2014.

25. Agarwal B. D., Broutman L. J., Chandrashekhara K., *Analysis and Performance of Fibre Composites*, third edition, John Wiley & sons, Inc., New Jersey, 2006.

26. Stratton A.L., Pelegri A., “Investigation of interlayer and intralayer delaminations, College of Engineering”, Rutgers University, Piscataway, NJ, 1999

27. Ding W., “Delamination Analysis of Composite Laminates”, University of Toronto, 1999.

28. Hull D. “A unifed approach to progressive crushing of fibre-reinforced composite tubes”, *Composites Science and Technology*, 40.4, pp. 377-421, 1991.

29. Jacob G. C., Fellers J. F., Starbuck M. J., Simunavic S., “Crashworthiness of automotive composite material systems”, *Journal of Composite Materials*, 36.7, 2003.

30. *ABAQUS Documentation*, Dassault Systèmes, Providence, RI, USA, 2011.

31. Hashin Z., "Failure criteria for unidirectional fibre composites", *ASME Journal of Applied Mechanics*, Vol. 47 (2), pp. 329-334, 1980.

32. Ladevéze P, Lubineau G. "On a damage mesomodel for laminates: micro–meso relationships, possibilities and limits", *Composite Science and Technology*, 61(15), pp. 2149–58, 2001.

33. Camanho P.P., Davila C.G., de Moura M.F., "Numerical simulation of mixed-mode progressive delamination in composite", *Materials Science, Composites*, 37(16), pp. 1415–38, 2003.

34. Chen J, Ravey E, Hallett S, Wisnom M, Grassi M. Prediction of delamination in braided composite T-piece specimens. *Composite Science and Technology*, 69(14), pp. 2363–7, 2009.

35. Chen J, New A. "Application of decohesive model with mixed damage scale infracture analysis of composite materials", *Journal of fatigue and fracture of engineering materials and structures,* 24(11), pp. 761–9, 2001.

36. Tvergaard V, Hutchinson J. W., "The relation between crack growth resistance and fracture progress parameters in elastic–plastic solids", *Journal of mechanical physics and solids,* 40(6), pp. 1377–97, 1992.

37. Turon A, Davila C. G, Camanho P.P., Costa J., **"**An engineering solution for mesh size effects in the simulation of delamination using cohesive zone models", *Engineering Fracture Mechanics*, 74, pp. 1665–1682, 2007.

38. Matzenmiller, A., Lubliner, J., and Taylor, R.L., "A Constitutive Model for Anisotropic Damage in Fibre-Composites," *Mechanics of Materials*, vol. 20, pp. 125-152, 1995.

39. CMH-17 meeting results. 6th CMH-17 Crashworthiness Working Group Meeting, Ottawa, CA; 5 August 2008

40. Haidong Y., Yongjin G., Xinmin L., "Rate-dependent behavior and constitutive model of DP600 steel at strain rate from 10-4 to 103 s-1" , *Materials and Design,* 30, pp. 2501–2505, 2009.

41. Hallett S.R., Green B.G., Jiang W.G., Wisnom M.R. "An experimental and numerical investigation into the damage mechanisms in notched composites", *Composites*, Part A 40, pp. 613–624, , 2009.

42. Türkiye İstatistik Kurumu, http://www.tuik.gov.tr/PreHaberBultenleri.do?id=21611, accessed August 2016